2012

Effect Of Childhood Obesity On Risk Of Pelvic Bone Fracture In Simulated Sideways Fall

Min-Heng Hsieh
University of Alabama at Birmingham

EFFECT OF CHILDHOOD OBESITY ON RISK OF PELVIC BONE FRACTURE IN SIMULATED SIDEWAYS FALL

by

MIN-HENG HSIEH

JONG-EUN KIM, COMMITTEE CHAIR
ALAN W. EBERHARDT
ALAN M. SHIH

A THESIS

Submitted to the graduate faculty of The University of Alabama at Birmingham,
in partial fulfillment of the requirements for the degree of
Master of Science in Mechanical Engineering

BIRMINGHAM, ALABAMA

2012

EFFECT OF CHILDHOOD OBESITY ON RISK OF PELVIC BONE FRACTURE IN SIMULATED SIDEWAYS FALL

MIN-HENG HSIEH

MASTER OF SCIENCE IN MECHANICAL ENGINEERING

ABSTRACT

Since the number of obese children in the U.S. has been increasing, the question arises whether obese children could be at higher or lower risk compared to nonobese children. The objective of this research was to investigate the risk of pediatric pelvic bone fracture in sideways falls using computational modeling and simulation considering various levels of obesity. Two sets of models were developed and tested. The first set was body component models. Several 10-year-old pelvis-femur complex models were developed. The models included biological soft tissue layers to reflect various levels of obesity, and they were validated against published experimental data. The second set was full body models in which the rest of body components were modeled by simple beams and mass elements for considering the whole body inertia. Sideways fall simulations were performed with the pelvis-femur complex models and full body models to see whether the cushion effect of the subcutaneous adipose tissue (SAT) layer or the momentum effect of whole body mass is more significant. A nonlinear explicit dynamic finite element code, LS-DYNA3D (LSTC, Livermore, CA) was used for model simulations. The simulation results indicate that the momentum effect of increased body mass of obese children would be more dominant over the cushion effect of the SAT layer.

Keywords: bone fracture, child obesity, computer modeling, finite element, pelvis

DEDICATION

To my family and my sincere friends.

ACKNOWLEDGEMENTS

This project was supported by the Nutrition Obesity Research Center (NORC) at the University of Alabama at Birmingham, through a grant from the National Institutes of Health (No. P30DK056336).

I greatly appreciate my advisor, Dr. Jong-Eun Kim, for his support, inspiration, and encouragement throughout my studies. I would like to thank him with my most sincere and deepest gratitude for his insights and timely advice guiding me towards appropriate research direction. Without his help, I would not have progressed this far. I also would like to express my deep gratitude to two committee members: Dr. Alan W. Eberhardt for his invaluable information and guidance, and Dr. Alan M. Shih for his help and precious comments.

My sincere thanks are due to a number of friends, Ruo-Hua He, Yangyang Hu, and Cheng-Chang Lee for their help, inspiration, and friendship.

My special thanks go to my family. Their spiritual support, encouragement, and understanding have made all the difference.

TABLE OF CONTENTS

Page

LIST OF TABLES

LIST OF FIGURES

Figure *Page*

LIST OF FIGURES (CONTINUED)

LIST OF ABBREVIATIONS

BMI	Body Mass Index
CDC	Centers for Disease Control and Prevention
CT	Computed Tomography
FE	Finite Element
FEM	Finite Element Methods
HST	Homogenous Soft Tissue
MRI	Magnetic Resonance Imaging
MVCs	Motor Vehicle Crashes
SAT	Subcutaneous Adipose Tissue
TST	Trochanteric SAT Thickness

CHAPTER 1

INTRODUCTION

In the United States, the prevalence of obese children has increased over 15% between 1963-2008, and approximately 17% of children and adolescents are considered obese [1]. A child whose body mass index (BMI) at or above the 95th percentile on the Centers for Disease Control and Prevention (CDC) growth charts is considered obese [2]. Even though there were no significant changes in the prevalence of childhood obesity in recent decades, the population of obese children and adolescents still increased steadily.

Obese Children and Body Injuries

For obese children, obesity can result in a variety of health problems, including obvious ones, such as diabetes and high blood pressure, and perhaps less obvious ones, such as a greater risk of injury in accidents. Because of their active lifestyles, children are always at risk of death and injury from accidents, including motor vehicle crashes (MVCs) and sports injuries. One injury in particular, a pelvic fracture, has multiple negative consequences for children, such as morbidity and disability. Therefore, current child protective and restraint systems might not be appropriate to prevent obese children from serious injury. Prior research pointed out that most hip fractures were due to sideways fall [3][4]. Some studies indicated the impact force was related to soft tissue thickness [5][6]. Low soft tissue thickness is a risk factor due to reduced energy absorption. A thicker soft tissue was able to provide efficient cushion effect [5]. Total

body height and impact velocity were also related to pelvis injury [7]. The amounts of body length and impact velocity can affect the degree of lateral rotation (rotating either the trunk or the pelvis sideways) of the pelvis during a sideways fall and produce a momentum effect toward the pelvis portion.

Considerable studies on adult pelvic injuries have been performed by use of adult cadavers, and their surrogates. However, experimental studies on pediatric pelvis have been very limited due to difficulties in acquiring child cadavers. Therefore, the risk and injury mechanism on pelvis for nonobese and obese children remains unexplained.

Few biomechanical and epidemiological studies have been conducted to investigate the relationship between childhood obesity and injury severity. Davidson et al. used a rheological-stochastic simulation model to explore the role of the biomechanical factors of impact force, bone strength, fall height, and surface stiffness on the risk of forearm fracture in obese and nonobese children [8]. The results showed that obese children had 1.7 times the risk of forearm fracture, compared to nonobese children. Also, the lower fall height and softer impact surface would not reduce the injury risk for obese children. A motor vehicle crash research used a probability sample of children who aged 9-15 years in 2000-2006 to determine the relationship between BMI and injury risk in motor vehicle crashes [9]. This study indicated that overweight and obese children are at increased risk of injury to the lower and upper extremities. Another study compared characteristics of injuries between obese and nonobese children in a pediatric emergency department [10]. This observation showed that obese children are more likely to sustain lower extremity injuries than upper extremity injuries. A study of chronic ankle morbidity in obese children (8-18 years old) by Nathan et al. revealed that children with a BMI in the 85th or

greater percentile for age were more likely to sustain persistent symptoms [11]. Bazelmans et al. observed the relationship between obesity and trauma among young people (9-17 years old) [12], and stated that they did not observe an association between obesity and severe injuries. They also noted that obesity as a risk factor for injuries has to be confirmed by other studies, and the understanding of the mechanism for the observed association needs more investigation.

Computational Simulation

To investigate the injury severity and mechanism of human body, cadavers, crash dummies, and computer models are utilized in experimental studies. The computational simulation is able to set up various testing scenarios and produce massive experimental data in a short period of time. Due to the convenience and efficiency of computational methods, computer crash simulation has become a valuable tool for design, testing, and improvement of safety systems. In comparison, cadaveric and dummy tests have a short lifetime that restricts the capability in experiments.

Objective

Although many epidemiological studies have been conducted examining the role of obesity and child injury severity, no computational model has been developed or tested for obese children. Moreover, the risk and mechanism of injury for obese children are still unknown. We hypothesized that a child with a higher BMI value would have a higher risk of bone injuries. More specifically, the purpose of this study was to investigate the risk of pelvic bone fracture sustained by obese children exposed to high-

speed impact environments. In particular, we also want to know which factor is more significant in causing the damage – the cushion effect or the momentum effect.

Approach

No physical surrogates for obese children are available, and experiments on pediatric cadavers are generally not probable. Therefore, our approach was to design computational simulation models based on a previously developed finite element (FE) model of a 10-year-old pelvic musculoskeletal system. Two sets of models were developed and implemented. The first set was body component models. Pelvis-femur complex models were developed, in which the flesh, organs, and subcutaneous adipose tissue (SAT) were modeled. The thickness of the SAT layer, which may play an important role in attenuating impact force (i.e., cushion effect), was adjusted to represent various levels of obesity. The models were validated against cadaveric experimental data provided by Ouyang et al. [28]. Sideways fall simulations were performed with the pelvis-femur complex models to mainly see the cushion effect of the SAT layer. A critical impact speed that yielded pelvic bone fracture was found and compared between the different levels of obesity. A nonlinear explicit dynamic finite element code, LS-DYNA3D (LSTC, Livermore, CA) was used for model simulations.

The second set was full body models. In order to account for the whole body inertia (referred to as ‘momentum effect’ in this study), the rest of body components except the pelvis-femur complex were modeled by simple beam and mass elements. Four models were developed. Their body mass indices (BMI) are 16.6, 19.6, 22.5 and 25.0, which are

50th, 85th, 95th, and over 97th percentile respectively, based on the age- and sex-specific BMI charts provided by the CDC in 2000.

CHAPTER 2

METHODS

Development of the Obese Pelvis Model

The purpose of this research was to explore and evaluate the association between 10-year-old obese child models and body injuries in sideways fall. A well-developed musculoskeletal FE model [13] of a 10-year-old child pelvis that includes bone structures and associated joint cartilages and ligaments was exploited in this study. The material constitutive model and properties are listed in Table 1. The musculoskeletal pelvis model was modified by attaching the biological tissue data to the architecture, and biomechanical properties were assigned to the biological soft tissue by FEM.

Table 1

Material constitutive models and properties for the musculoskeletal, skin, SAT, and HST of a 10-year-old child pelvis

Components	Constitutive model	Properties	References
Cortical bone	Elastic-plastic	Young's modulus: 12.24 Gpa Poisson's ratio: 0.3 Average thickness: 1.6 mm Yield strength: 150 MPa Failure strain: 0.027	13 14
Trabecular bone	Elastic-plastic	Young's modulus: 44.8 MPa Poisson's ratio: 0.2 Yield strength: 7.5 MPa Failure strain: 0.25	13 14
Interpubic joint cartilage	Hyperelastic (Monney-Rivlin)	C_{10}=0.07 MPa, C_{01}=0.315 MPa, C_{11}=0.42 MPa	13, 15
Sacroiliac joint cartilage	Hyperelastic (Monney-Rivlin)	Two parametric C_1=2.87 MPa, C_2=0.287 MPa	13, 16
Hip joint cartilage	Hyperelastic (Monney-Rivlin)	Two parametric C_1=2.87 MPa, C_2=0.287 MPa	13, 16
Interpubic ligament	4 spring elements	Spring constant: 0.38 kN/mm	13, 17
Sacroiliac ligament	16 discrete truss elements	Young's modulus: 140 MPa Area: 224 mm^2	13, 18
Hip ligament	18 discrete truss elements	Young's modulus: 127 MPa Area: 210 mm^2	13, 19
Sacrospinous ligament	12 spring elements	Spring constant: 1.05 kN/mm	13, 20
Sacrotuberous ligament	12 spring elements	Spring constant: 1.05 kN/mm	13, 20
Skin	Elastic	Young's modulus: 420 kPa Poisson's ratio: 0.45 Thickness: 2 mm Density: 1200 kg/m^3	21 22 23 24
SAT	Viscohyperelastic	C_1: 6.33 kPa, C_2: 1.58 kPa[a] G_1: 0.50 kPa, G_2: 2.20 kPa[b] β_1: 0.54, β_2: 0.06[c] Density: 900 kg/m^3	25 26
HST	Viscohyperelastic	C_1: 21.5 kPa, C_2: 5.37 kPa G_1: 1.72 kPa, G_2: 7.53 kPa β_1: 0.54, β_2: 0.06 Density: 1200 kg/m^3	

Abbreviations: SAT, subcutaneous adipose tissue; HST, homogeneous soft tissue.
[a]C_2=0.25 C_1 [27].
[b]G_1 and G_2 are shear relaxation modules.
[c]β_1 and β_2 are decay constants.

Generation of Musculoskeletal Model Surface Mesh

Based on the developed child pelvis musculoskeletal model, a series of models with various levels of obesity were constructed. The first step was to retrieve bone surface data by parts, such as sacrum, ilium, ischium, and pubis. However, the geometry of the human pelvis is rough and irregular, which might affect the accuracy of surface data. To reduce the error impact, some surface data would be extracted piece by piece according to the curvature of bone surfaces. When all the surfaces were built (Figure 1), the next step was to eliminate duplicated intersurfaces between each pelvis component (Figure 2). After removing the duplicated intersurfaces, there were many free edges (shown in red lines), which indicated that some surfaces were not enclosed (Figure 3a). In order to generate a completely enclosed bone surface mesh, gaps between each part of open surfaces were sealed by applying the replacing lines function in Hypermesh (Figure 3b). When every part of musculoskeletal model surfaces was connected, the number of surface mesh elements was adjusted by modifying and removing control points and control lines (Figure 4). The purpose of this process was to reduce the computation time while rendering a competitive representation of bone surface model. Another problem was that the posture of femurs did not match the skin data. Due to this mismatch issue, the femur sections were rotated 90 degrees for fitting in the human skin data (Figure 5). Similarly, the pelvis surface FE mesh could be done as well (Figure 6).

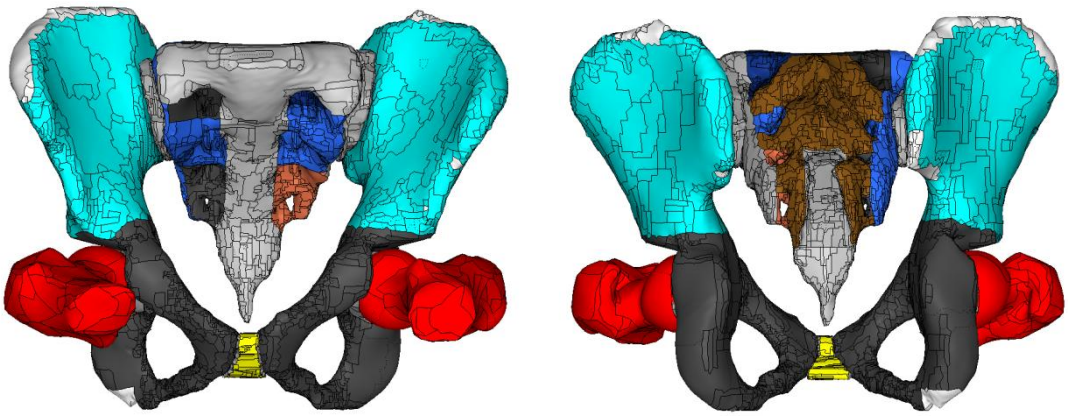

(a) (b)

Figure 1. Retrieved surface data from bone structure: (a) front view (b) back view.

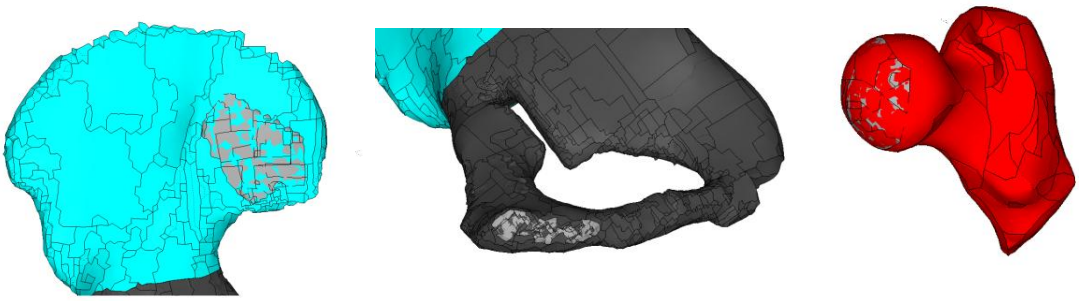

(a) (b) (c)

Figure 2. Duplicated surfaces between (a) ilium and sacroiliac joint (b) pubic bone and pubic symphysis (c) femur and hip joint cartilage.

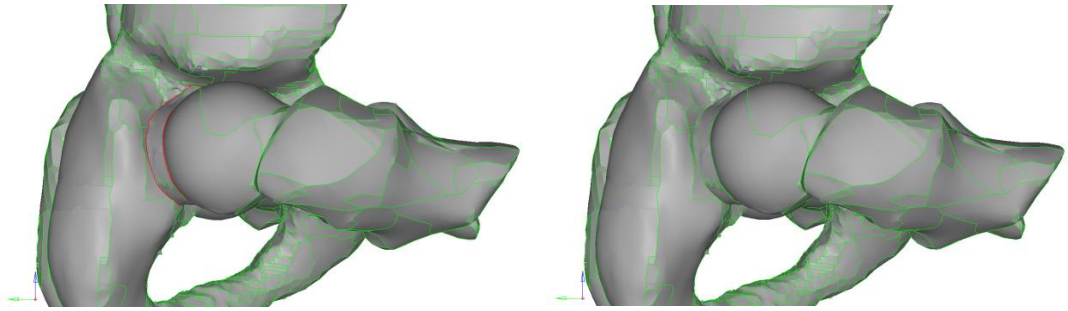

(a) (b)

Figure 3. The surfaces between femur, hip joint cartilage, and ilium are (a) not connected (b) connected.

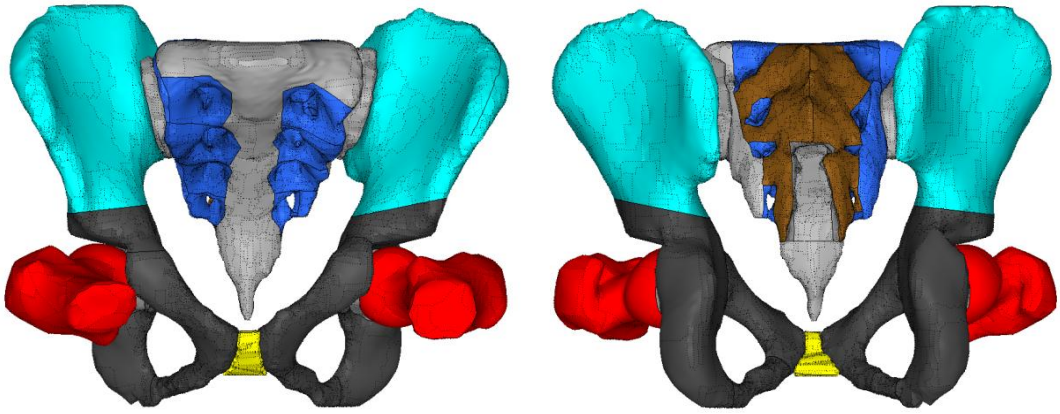

(a) (b)

Figure 4. Retrieved surface data from bone structure: (a) front view (b) back view.

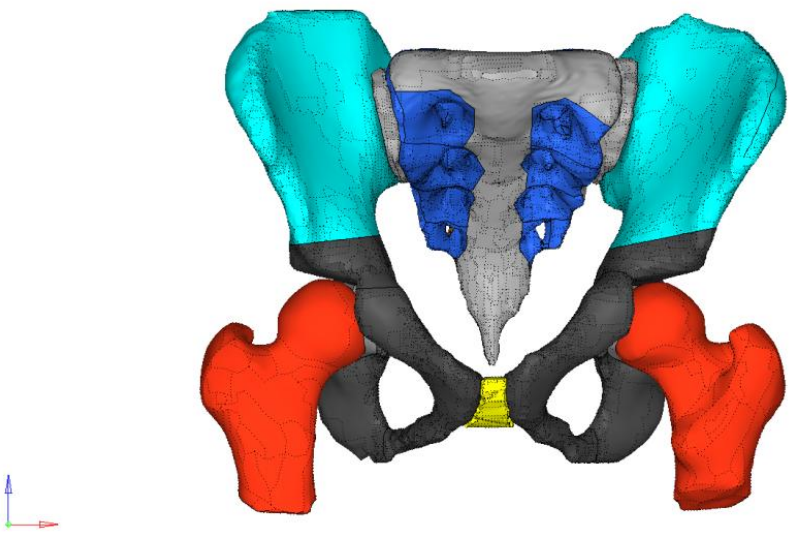

Figure 5. The femur is rotated 90 degrees.

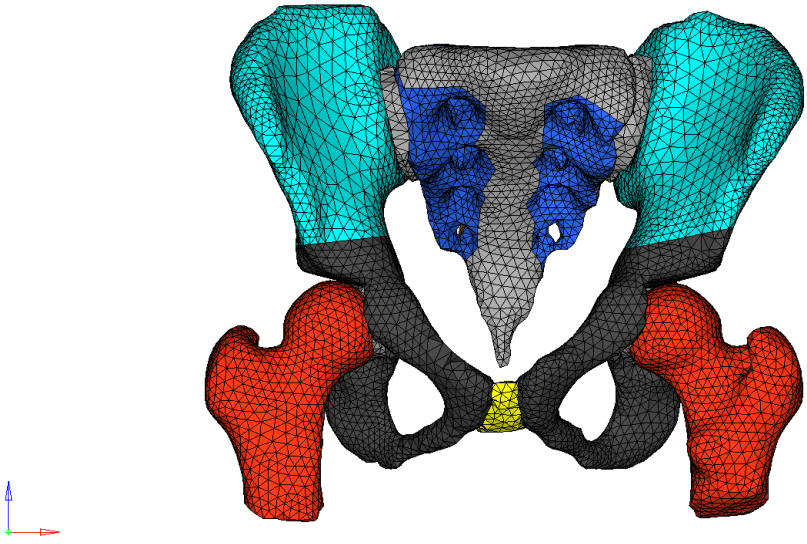

Figure 6. Completely enclosed pelvis-femur complex surface FE mesh.

Development of the Biological Soft Tissue Mesh

After the pelvis surface FE mesh was generated, the next step was to adjust the relative position between bone surface FE mesh and skin FE mesh. The skin mesh data, which were from a computed tomography (CT) scan obtained from the previous study [13] was imported to Hypermesh software (Altair Engineering, Inc., Troy, MI) to make a surface mesh. In order to reduce the computation time, the part that was associated with this study was trimmed. Thus, the number of skin mesh elements was reduced to 838 triangle elements (Figure 7). The biological tissue mesh could be constructed by filling the enclosed space between the bone surface mesh and the skin mesh (Figure 8).

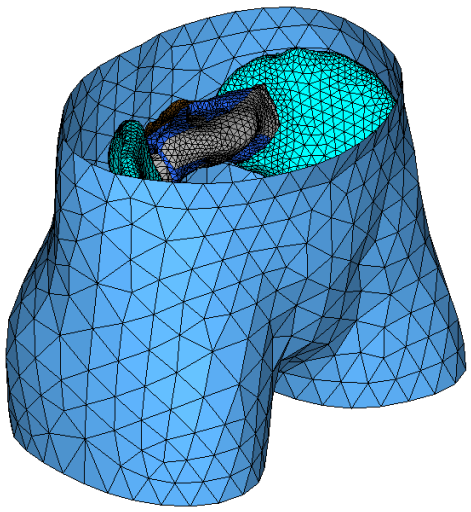

Figure 7. The skin mesh with bone surface FE model.

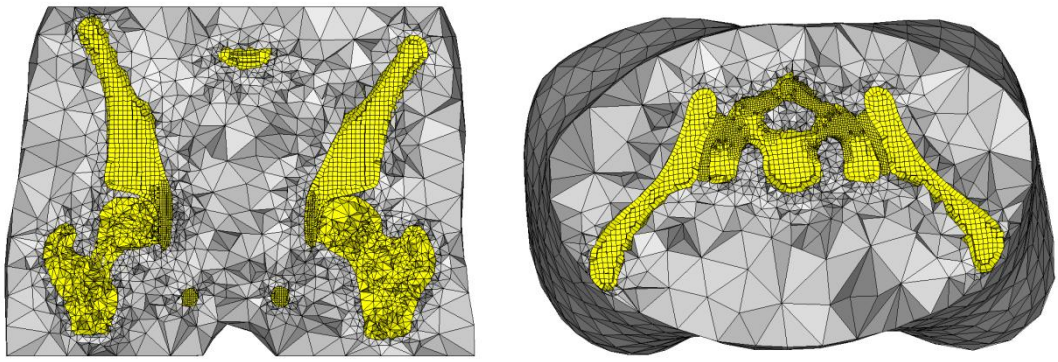

Figure 8. Tetrahedral soft tissue FE mesh based on an existing skin mesh and pelvis surface mesh with different aspects.

Different Levels of Obesity Modeling

In this study, two layers of biological tissue were considered. The first layer with 86,576 tetrahedrons was a homogeneous soft tissue (referred to as HST in this study), including skeletal muscle, internal organs, and visceral adipose tissue. The second layer with 2,514 tetrahedrons was a subcutaneous adipose tissue (SAT). This model is referred to as a "normal model" in this study, whose nominal SAT thickness is 3.6 mm (Figure 9a). By gradually increasing SAT thickness, three more different levels of obesity models were developed. The nominal trochanteric SAT thickness (TST) is 3.6, 8.6, 16.3, and 24.7 mm for the total weights of the pelvis-femur complex 7.04, 7.45, 8.23, and 8.88 kg, respectively (Figure 9).

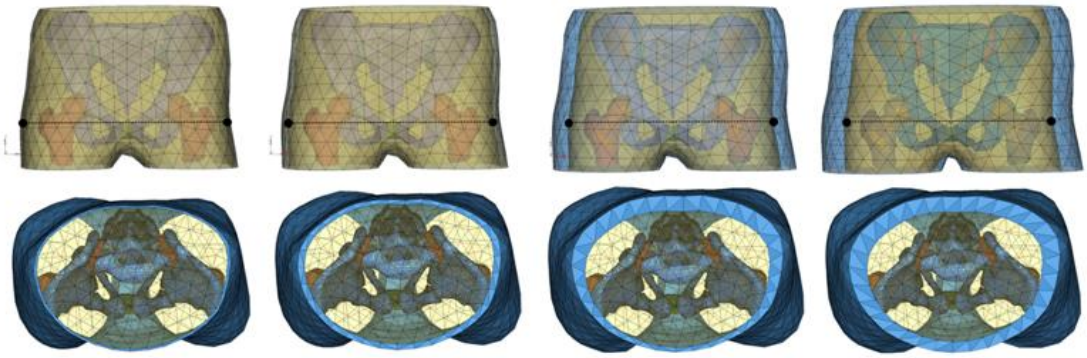

(a) (b) (c) (d)

Figure 9. The FE model of pelvis-femur-soft tissue complex of (a) normal model, TST = 3.6 mm, (b) TST = 8.6 mm, (c) TST = 16.3 mm, and (d) TST = 24.7 mm.

Material Properties for the Soft Tissues (skin, SAT, and HST) and Model Validation

A hyperelastic material model with viscous effect was applied to HST and SAT for a better representation of the human soft tissues [25][26]. An elastic material was used for the skin in the model simulation [13]. The cadaveric experiments conducted by Ouyang et al. [28] were used for model validation. In their experiments, the torso and head of a child cadaver were fixed on a flank, and the legs were in free position. The pelvises of the child cadaver were laterally impacted by a flat plate from the right side, and the left side was against a supporter. Impact force and pelvic viscous criteria (pelvic compression times velocity of deformation) were measured. In this study, an FE model was created to replicate the experiments, and computational analyses were performed for model validation (Figure 10). A normal model (Figure 9a) was used in comparison with the experimental data for model validation.

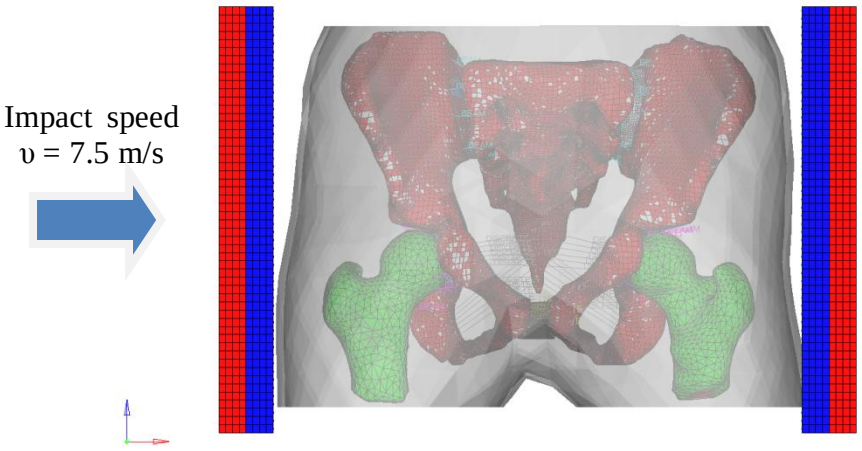

Figure 10. The FE model developed according to the cadaveric experiments for model validation.

Model Simulation Using the FE Code LS-DYNA3D

A nonlinear explicit dynamic FE code of LS-DYNA3D (LSTC, Livermore, CA) [29] was used for model simulation in this study. Bone fracture was simulated by using an element eroding option, in which FEs whose strains exceed a failure strain are eroded [29]. When an element is stressed over the yield stress, the element is easily deformed and yielded to reach the predefined failure strain. Such elements are then eroded and lose the element connectivity so that bone fracture can be observed (Figure 11). The contact interface had to be defined in LS-DYNA3D as well; otherwise, the objects that should be contacted would be penetrated. Also, automatic tiebreak contacts behaved as automatic contacts after failure. Therefore, a tiebreak contact was defined between pelvis-femur complex and HST. The tiebreak contact commend of LS-DYNA3D was shown in Figure 12. The automatic contact surface was defined between floor and skin, and floor and SAT. The same interface nodes were used between SAT and HST (i.e., node sharing), so that the SAT and HST were contacted automatically.

Figure 11. Elements eroding option was applied to simulate bone fracture.

```
*CONTACT_TIEBREAK_SURFACE_TO_SURFACE_ID
$HMNAME GROUPS       18cortical-hipL shell
$HWCOLOR GROUPS       18        4
$       CID
         10
$      SSID       MSID      SSTYP      MSTYP     SBOXID     SBOXID
         1         50          3          3          0          0

$      NFLS       SFLS
        1.0        0.5
```

Figure 12. LS-DYNA3D commend for tiebreak contact. CID is contact ID, SSID is slave segment ID, (the number 1 indicates pelvis cortical bone), MSID is master segment ID, (the number 50 indicates left hip joint), SSTYP is slave segment type, (3 means the number of SSID is part ID), MSTYP is master segment type, NFLS is tensile failure stress, and SFLS is shear failure stress.

Free Fall Simulation of the Body Component (pelvis-femur complex)

To simulate a free fall from a fixed height (h = 0.5) with different TST, a certain impact speed (v), 3.13 m/s ($v = \sqrt{2gh}$, where g is the acceleration of gravity, 9.8 m/s^2), was applied against a floor (Figure 13). The floor was modeled by a rigid plate as a

baseline. The mechanical responses (impact force, deformation, viscous criteria, stress, and energy) were measured. Then, the impact speed was adjusted in a certain range to find a critical impact speed that yielded pelvic bone fracture. A highly compressive low-density foam material constitutive model [29] was used and the material constants were adjusted to represent soft, medium, stiff, and rigid floors. A total number of 16 simulations were created to examine the association between obesity, bone fraction, and floor properties as shown in Table 2.

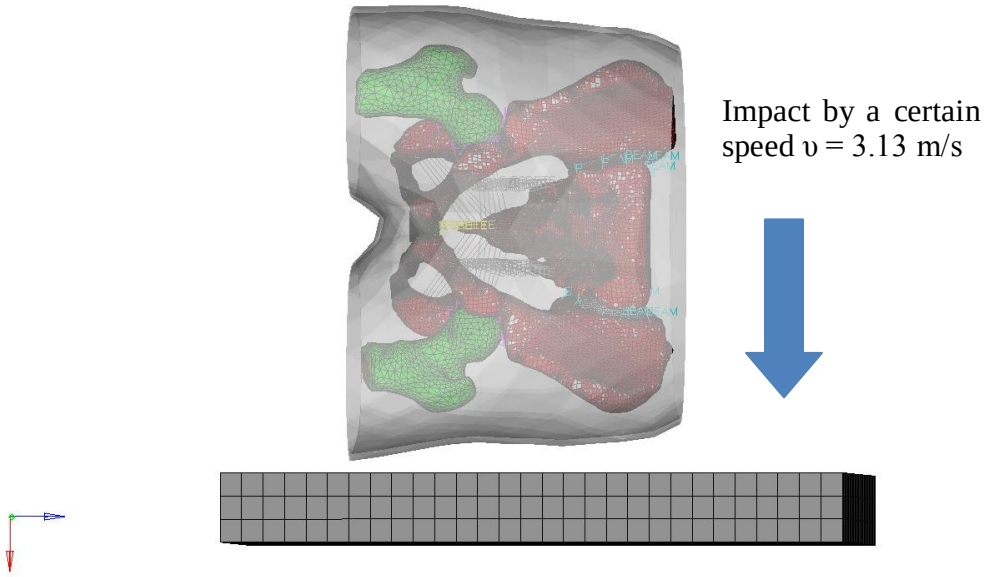

Figure 13. Free fall simulation by using an impact speed υ = 3.13 m/s on normal model, TST = 3.6 mm.

Table 2

Variables for pelvis-femur complex free fall simulation and case studies

Floor properties	TST = 3.6 mm	TST = 8.6 mm	TST = 16.3 mm	TST = 24.7 mm
Rigid	Case 1-1	Case 1-2	Case 1-3	Case 1-4
Stiff	Case 2-1	Case 2-2	Case 2-3	Case 2-4
Medium	Case 3-1	Case 3-2	Case 3-3	Case 3-4
Soft	Case 4-1	Case 4-2	Case 4-3	Case 4-4

Simple Full Body Model Development

For considering the full body inertia effect on pelvic bone injury, a simple full body model was developed. According to a national health statistics report [30], which included average weight, height, upper arm length, and several useful human body measurements of children and adolescents, we are able to find the average height and weight of 10-year-old children from this statistics report. However, we need body segment parameters as well to build full body FE models. By considering the published sources of pediatric body segment parameters [31-33] and modifying the adult body segment parameters [34] by the ratio of height and weight, a body segment parameters table for a 10-year-old child was established (Tables 3 and 4).

Table 3

Body mass distribution

Model	50th percentile	85th percentile	95th percentile	97th percentile	References
BMI	16.6	19.6	22.55	25	
Height, cm	142.3	142.3	142.3	142.3	30
Weight, kg	33.61	39.69	45.66	50.62	
Head, kg	3.70 (11.0)[1]	3.97 (10.0)	4.11 (9.0)	4.30 (8.50)	31
Upper and Mid Trunk, kg	10.65 (31.7)	13.75 (34.7)	16.62 (36.4)	18.91 (37.4)	34
Upper Arms, kg	1.61 (4.8)	2.06 (5.2)	2.47 (5.4)	2.83 (5.6)	31
Forearms, kg	0.94 (2.8)	1.11 (2.8)	1.28 (2.8)	1.42 (2.8)	31
Hands, kg	0.61 (1.8)	0.64 (1.6)	0.64 (1.4)	0.63 (1.2)	31
Thighs, kg	4.71 (14.0)	5.56 (14.0)	6.39 (14.0)	7.09 (14.0)	32
Shanks, kg	3.36 (10.0)	3.97 (10.0)	4.57 (10.0)	5.06 (10.0)	32
Feet, kg	1.00 (3.0)	1.18 (3.0)	1.36 (3.0)	1.50 (3.0)	33
Sum (Except pelvis-femur complex), kg	26.57 (79.0)	32.24 (81.2)	37.44 (82.0)	41.74 (82.5)	
Pelvis-femur complex, kg	7.038 (21.0)	7.452 (18.8)	8.225 (18.0)	8.882 (17.5)	

[1]pecentage (mass/total mass *100)

Table 4

Body length parameters

	Length (cm)	References
Head	16.62	34
Upper and Mid Trunk	31.57	34
Thigh	34.6	30
Shank	35.47	34
Foot	2	
Upper Arm	22.9	34
Forearm	21.8	34
Hand	5.57	34

When all the body parameters were decided, a simple body structure was constructed by Hypermesh software (Altair Engineering, Inc., Troy, MI). Mass elements, continuous beams, or discrete beams [35] were chosen for different body portions (Table 5). Each body part was represented by a single beam element except torso and femur parts. Multiple beams were used for torso and femur to enhance the stability of body structure (Figure 14). All beams were assumed as cylinders, and mass elements were used on head, hands, and feet. The whole body was set parallel to the floor. Four models were developed for the BMI of 50th, 85th, 95th, and over 97th percentiles, respectively (Figure 15), based on the age- and sex-specific BMI charts provided by the CDC in 2000. A certain impact speed, 1.9 m/s was used on full body simulation for measuring the mechanical responses. Similar as the pelvis-femur complex cases, the impact speed was adjusted for finding a critical impact speed that yielded pelvic bone fracture. Similarly, 16 simulations were developed to examine the association between BMI, and bone fraction with different floor properties as shown in Table 6. The mechanical responses and critical impact speeds that fractured the bone were measured. These simulations with

the full-body model could examine the momentum effect of a greater body mass as a result of obesity.

Table 5

Element quality list of body components

Component	Quality of element
Head	Mass element
Upper and Mid Trunk	Continuous beam
Thigh	Continuous beam
Shank	Spring element
Foot	Mass element
Upper Arm	Discrete element
Forearm	Discrete element
Hand	Mass element

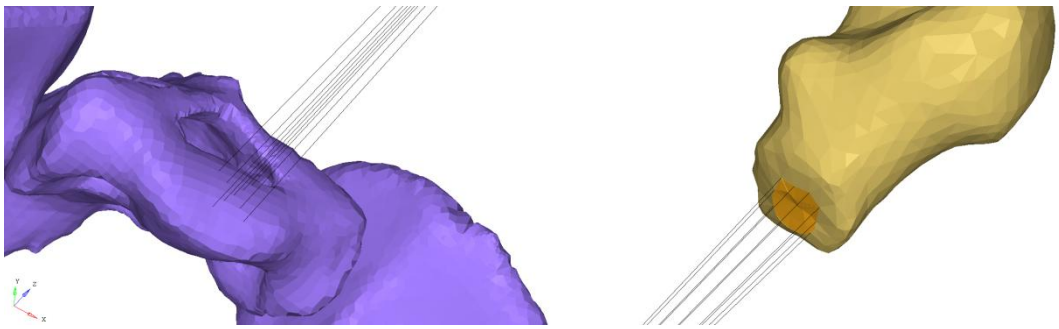

(a) (b)

Figure 14. Multiple continuous beams were applied to enhance the strength of connection: (a) connection between torso and sacrum (b) connection between femur bone mesh and femur beams.

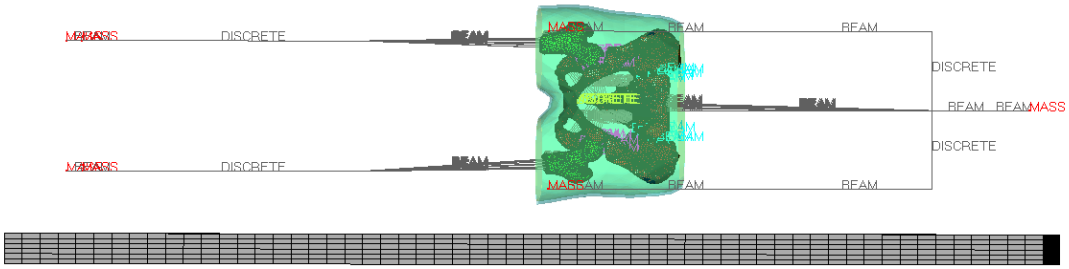

(a)

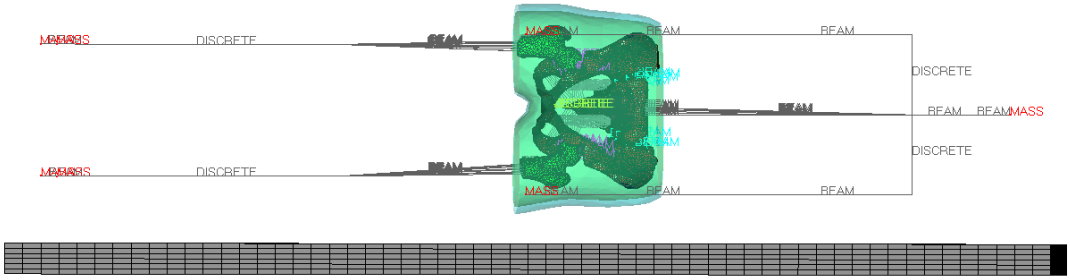

(b)

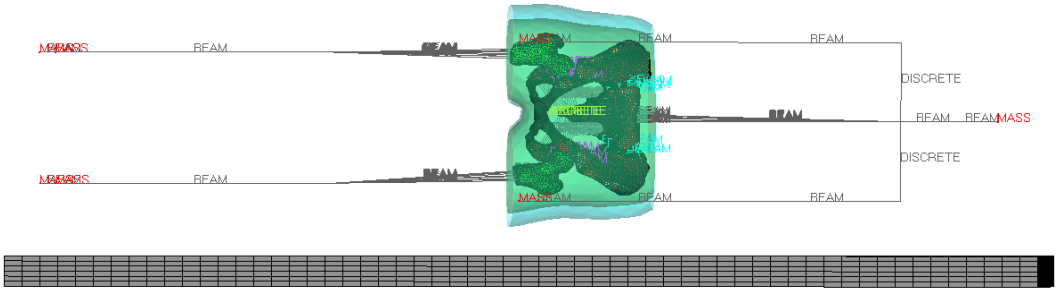

(c)

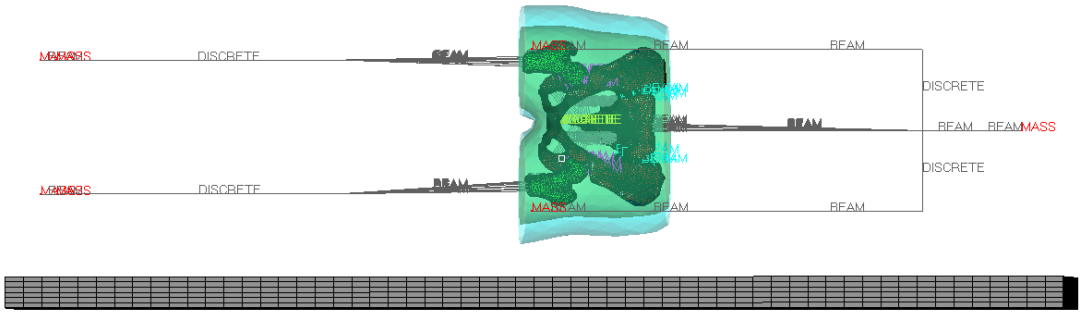

(d)

Figure 15. Simple full body models of (a) BMI = 50th, (b) BMI = 85th, (c) BMI = 95th, and (d) BMI = 97th.

Table 6

Variables of the full body model for free fall simulation and case studies

Floor properties	50^{th} percentile	85^{th} percentile	95^{th} percentile	97^{th} percentile
Rigid	Case 5-1	Case 5-2	Case 5-3	Case 5-4
Stiff	Case 6-1	Case 6-2	Case 6-3	Case 6-4
Medium	Case 7-1	Case 7-2	Case 7-3	Case 7-4
Soft	Case 8-1	Case 8-2	Case 8-3	Case 8-4

CHAPTER 3

RESULTS

LS-DYNA Simulation

Model Validation

Several mechanical responses, such as viscous criteria, force, and displacement were measured and calculated using the model depicted in Figure 10. A series of images captured from the simulation with stress distribution for model validation are shown in Figure 16. Pictures were captured every 10 milliseconds (ms) over a time span of 50 ms. The simulation data were compared with those of cadaveric experiments provided by Ouyang et al. [28], and the results are shown in Figure 17. It was obvious that the distributions of cadaveric experimental data and simulation results were pretty similar. No injury was induced in cadaveric experiments under velocity at 7.5 ±0.5 m/s [28]. There was no pelvic fracture in model simulation as well.

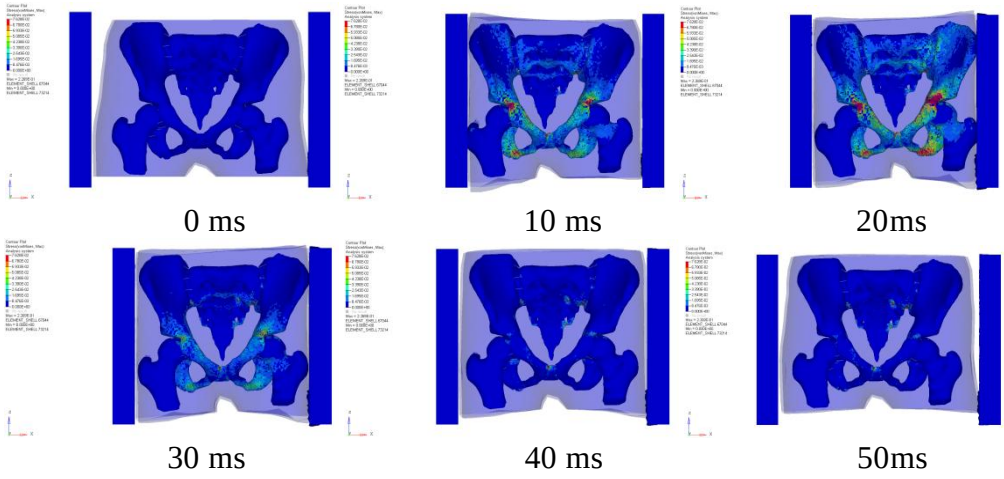

Figure 16. Images of model validation by a time step of 10 ms over a span of 50 ms.

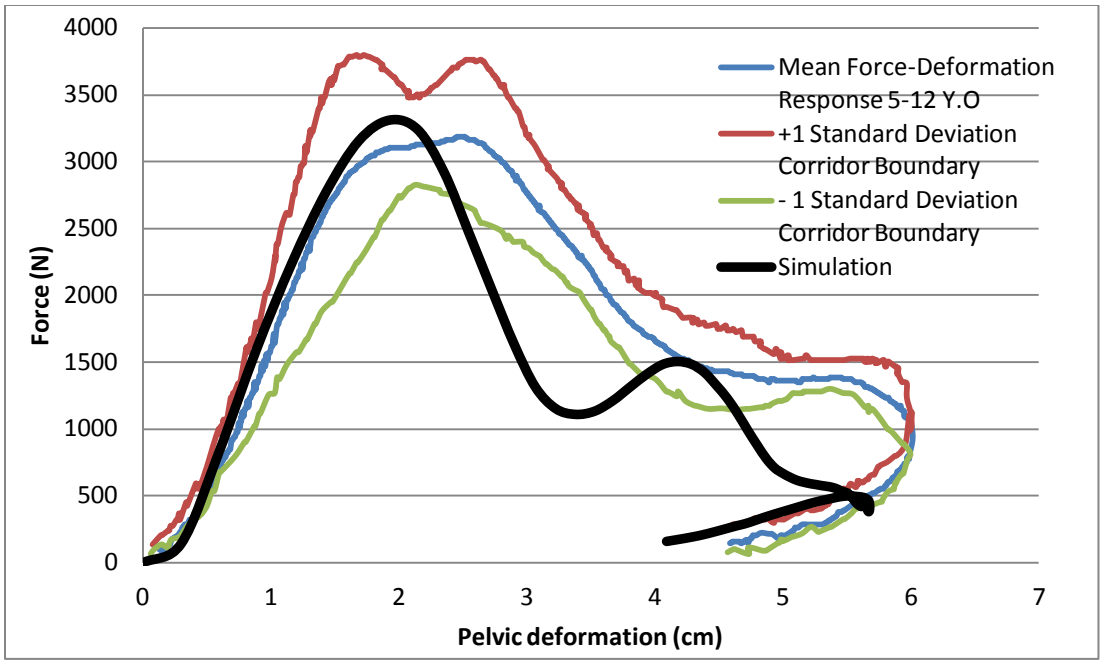

(a)

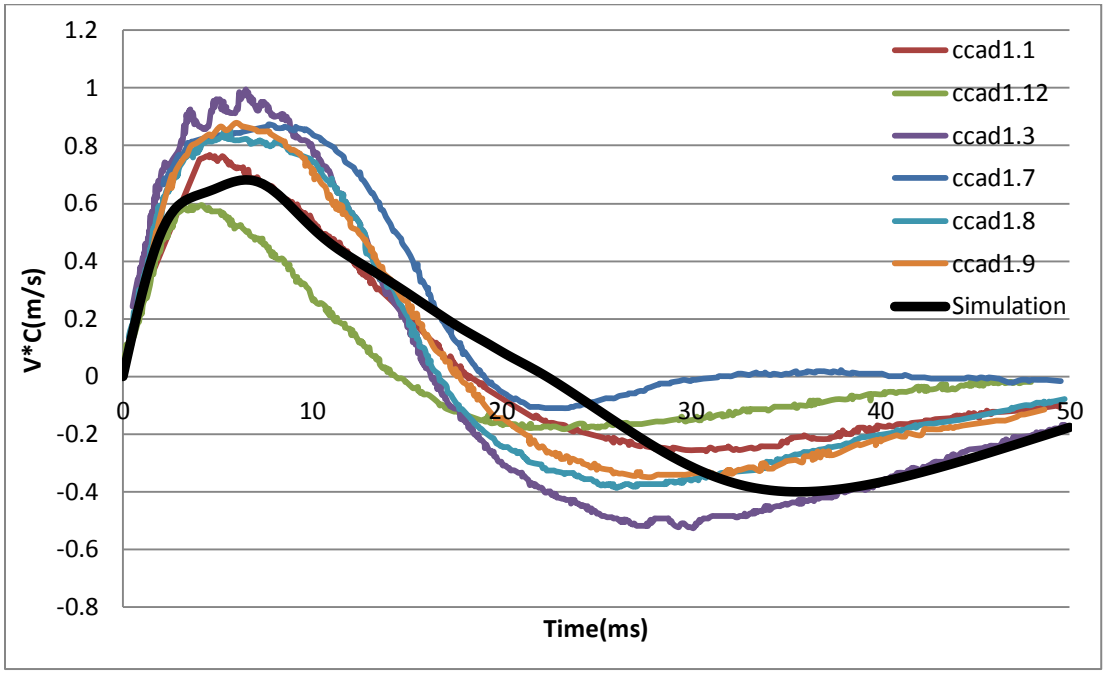

(b)

Figure 17. Model Validation. The black line indicates the result of simulation. All curves other than the black line are from the experimental data by Ouyang et al. [28]: (a) Impact force versus pelvic deformation (b) Viscous criteria versus time.

Sideways Fall Simulations: Pelvis-Femur Complex

Under a certain speed υ =3.13 m/s, impact force, viscous criteria, and strain energy were calculated for the pelvis-femur complex model. The impact force was measured from the contact force between the soft tissue and the floor. The measuring points to calculate the viscous criteria are indicated in Figure 9. The results of impact force, viscous criteria, and strain energy are shown in Figure 18. The von-Mises stress [36] was concerned in this study. Therefore, some spots on the cortical bone, such as iliac crest, iliac fossa, greater trochanter, femoral neck, femoral head, acetabulum, superior pubic ramus, ischiopubic ramus, inferior pubic ramus, ischial tuberosity, sacrum, and coccyx, were selected for analyzing the distribution of the von-Mises stress (Figure 19). Fifteen elements around each measuring spot were chosen to gain average stress, which is called the "15 contiguous element criterion" [37]. The value on each spot is listed in Table 7. The highest stress was on the impact-side inferior pubic ramus. It was observed in Table 7 that all stresses were less than the yield stress of cortical bone (150 MPa). Therefore, no bone fractures in this case.

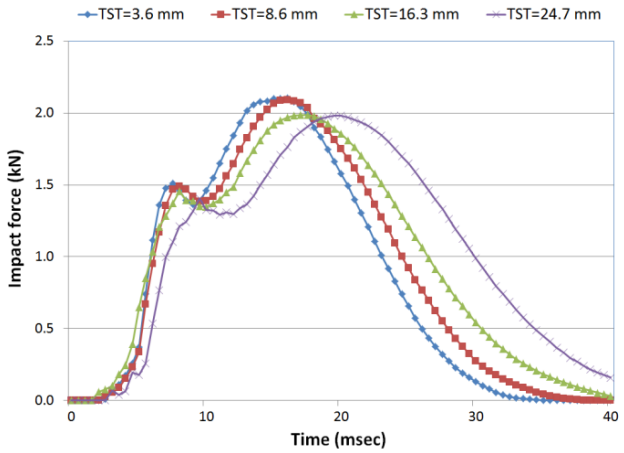

(a)

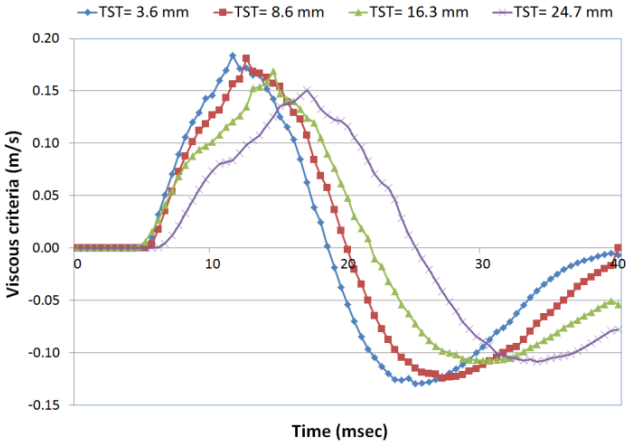

(b)

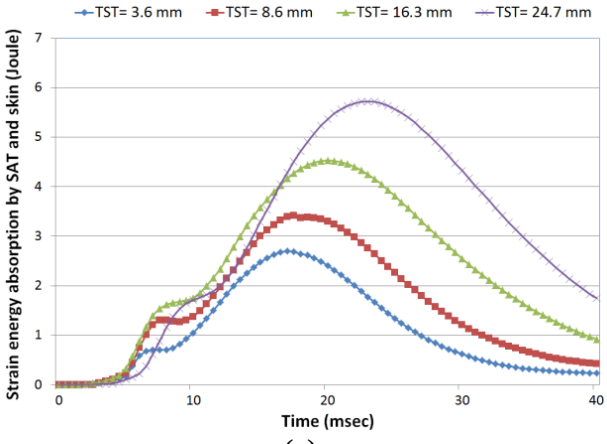

(c)

Figure 18. Results of sideways fall simulation using the pelvis-femur complex model: (a) impact force (b) viscous criteria (c) strain energy absorbed by SAT and skin.

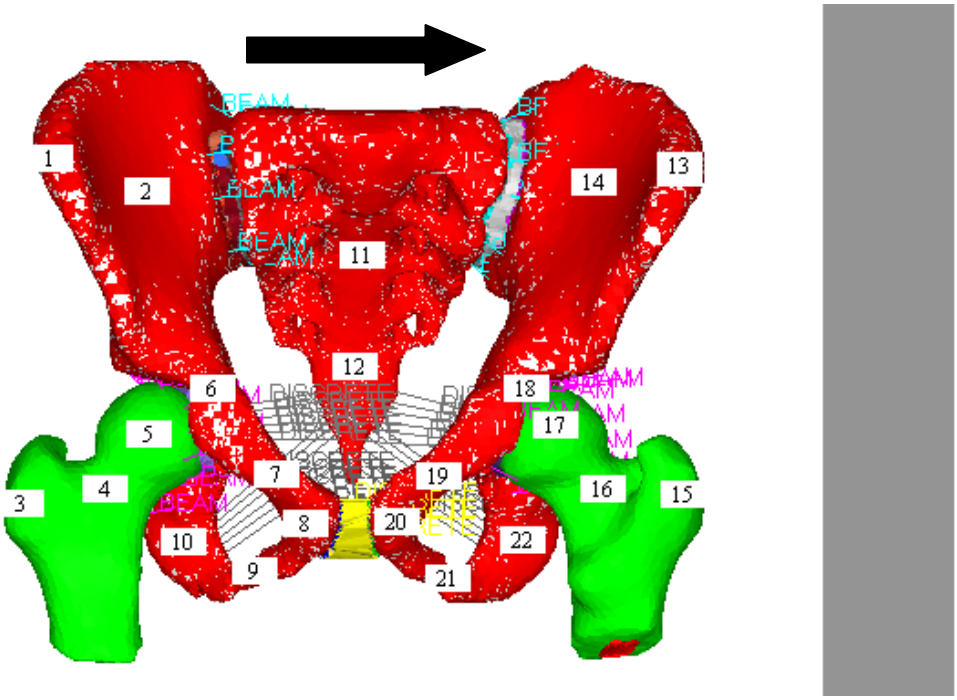

Figure 19. Measuring spots for bone stress. 1 and 13: iliac crest, 2 and 14: iliac fossa, 3 and 15: greater trochanter, 4 and 16: femoral neck, 5 and 17: femoral head, 6 and 18: acetabulum, 7 and 19: superior pubic ramus, 8 and 20: ischiopubic ramus, 9 and 21: inferior pubic ramus, 10 and 22: ischial tuberosity, 11: sacrum, and 12: coccyx.

Table 7

Maximum stress (MPa) at the measuring spots of the pelvis-femur complex model

Measuring spot	Model			
	TST=3.6 mm	TST=8.6 mm	TST=16.3 mm	TST=24.7 mm
1	1.54	1.64	1.43	1.67
2	2.02	2.00	2.04	1.89
3	0.85	0.88	0.91	0.90
4	9.29	9.31	9.42	9.19
5	3.27	3.23	3.37	3.40
6	18.69	18.76	18.70	18.07
7	28.78	28.45	26.73	26.62
8	15.95	15.68	15.03	14.92
9	36.65	37.12	34.73	32.28
10	23.67	23.41	22.36	22.17
11	7.38	6.85	6.67	6.35
12	4.58	4.21	5.26	5.00
13	10.74	9.46	7.21	6.17
14	5.25	5.17	3.29	3.37
15	2.85	2.53	2.53	2.55
16	22.11	22.23	21.48	21.72
17	5.92	5.88	5.71	5.64
18	20.97	20.76	19.75	19.55
19	38.09	37.43	34.04	33.92
20	16.63	16.31	15.12	15.02
21	60.57	59.57	55.31	56.02
22	34.50	33.98	32.28	31.95

To find the critical speed (a minimum impact speed that yielded bone fracture), the impact speed was adjusted within a certain range. While reaching a certain impact speed, some elements around inferior pubic ramus were eroded. The bone fracture at the moment was observed. All the critical speeds of 16 simulations in Table 2 were found, as shown in Figure 20. The mean values and standard deviations of the critical speeds are

depicted in the Figure 21. Figure 22a shows a series of pictures of sideways fall simulation under the critical speeds by using TST = 3.6 mm model. As shown in Figure 22b, the inferior pubic ramus fractures at 20 ms. The simulation results of the other cases are shown in the Appendix.

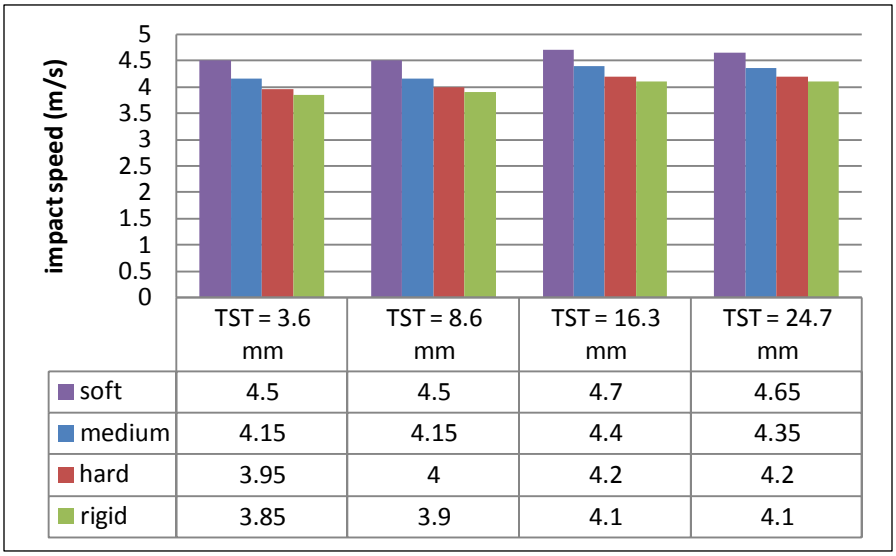

	TST = 3.6 mm	TST = 8.6 mm	TST = 16.3 mm	TST = 24.7 mm
soft	4.5	4.5	4.7	4.65
medium	4.15	4.15	4.4	4.35
hard	3.95	4	4.2	4.2
rigid	3.85	3.9	4.1	4.1

Figure 20. The critical speeds of different models and plate properties in the pelvis-femur complex model.

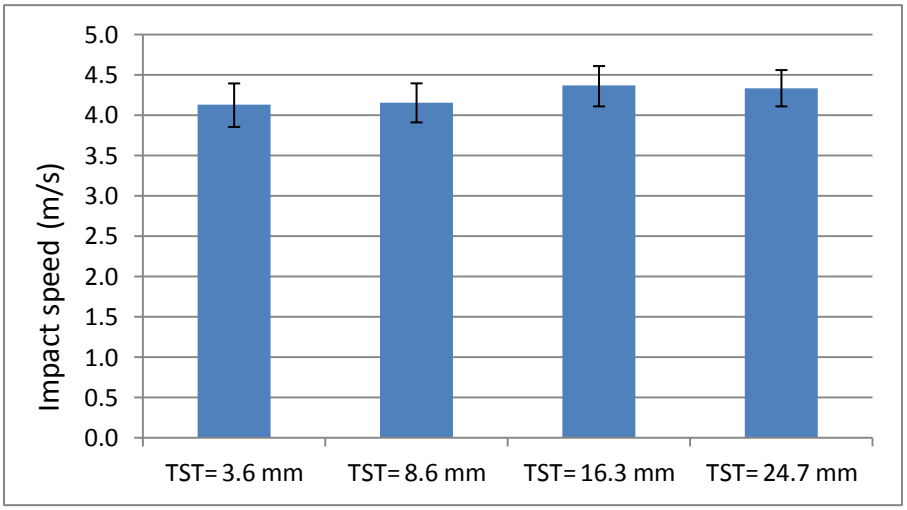

Figure 21. The mean values and standard deviations of the critical speeds in the pelvis-femur complex model.

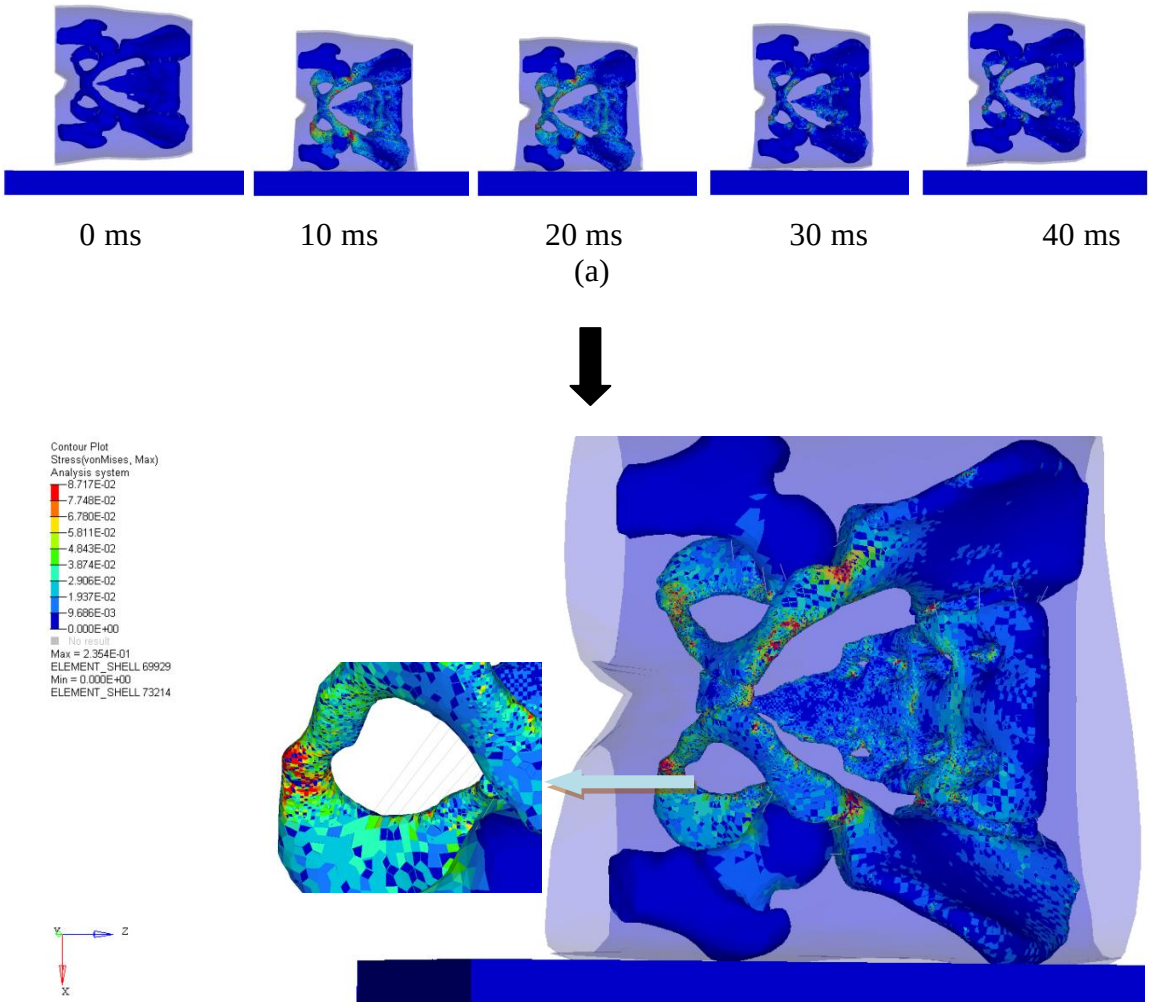

Figure 22. Images of sideways fall simulation of the pelvis-femur complex model: (a) by a time step of 10 ms (b) clear bone fracture snapshot.

Sideways Fall Simulations: Full Body

Under a certain speed υ =1.9 m/s, impact force, viscous criteria, and strain energy were measured for the full body model (Figure 23). Like the pelvis-femur complex model, the bone maximum stress distribution for the full body model was acquired (Table 8). The critical impact forces were then found for 16 simulations (Table 6) by arranging the impact speed. The mean values and standard deviations of the critical speeds are

shown in Figures 24 and 25. A series of snapshots of full body movement of the 50th percentile model are shown in Figure 26. An image at the moment of bone fracture is shown in Figure 27. The simulation results of the other cases are shown in the Appendix.

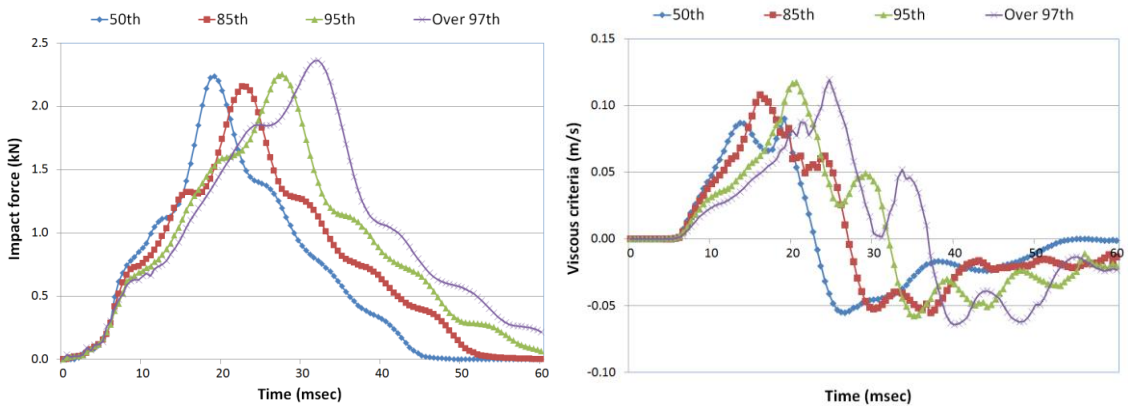

(a) (b)

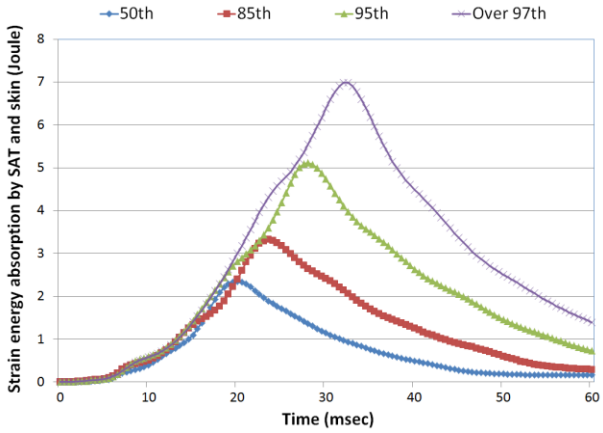

(c)

Figure 23. Results of sideways fall simulation using the full body model: (a) impact force (b) viscous criteria (c) strain energy absorbed by SAT and skin.

Table 8

Maximum stress (MPa) at the measuring spots of the full body model

Measuring spot	Model			
	50th	85th	95th	97th
1	3.54	2.40	2.85	2.75
2	8.72	8.92	8.44	10.16
3	9.40	9.28	9.03	9.37
4	33.40	39.22	35.28	40.37
5	11.11	17.47	18.40	18.34
6	28.71	29.63	39.89	45.91
7	26.58	29.59	30.80	32.17
8	15.77	16.00	16.69	17.03
9	43.42	37.32	43.21	45.63
10	26.64	27.76	31.90	33.53
11	11.28	11.33	12.45	12.60
12	10.69	10.74	11.60	10.45
13	14.41	7.90	6.61	6.33
14	9.49	8.58	12.76	10.71
15	8.24	6.46	4.91	4.48
16	45.49	37.93	37.69	31.36
17	10.88	8.70	7.90	6.00
18	18.92	16.96	20.45	17.08
19	34.00	36.93	38.73	41.41
20	19.90	19.04	20.03	20.77
21	54.83	66.77	67.91	69.61
22	33.06	34.07	34.49	33.73

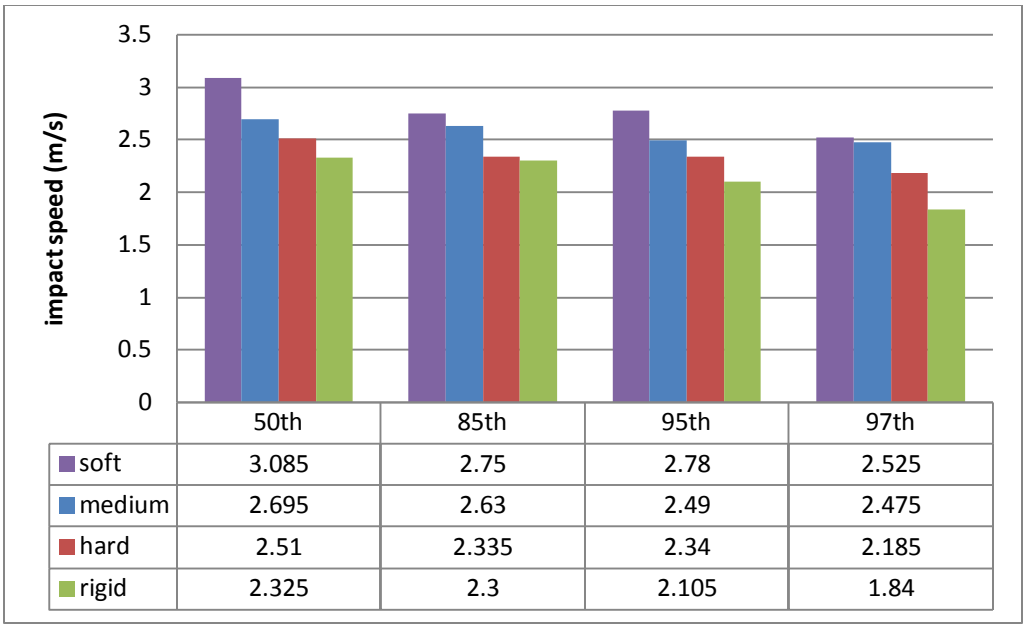

	50th	85th	95th	97th
soft	3.085	2.75	2.78	2.525
medium	2.695	2.63	2.49	2.475
hard	2.51	2.335	2.34	2.185
rigid	2.325	2.3	2.105	1.84

Figure 24. The critical speeds of different models and plate properties in the full body model.

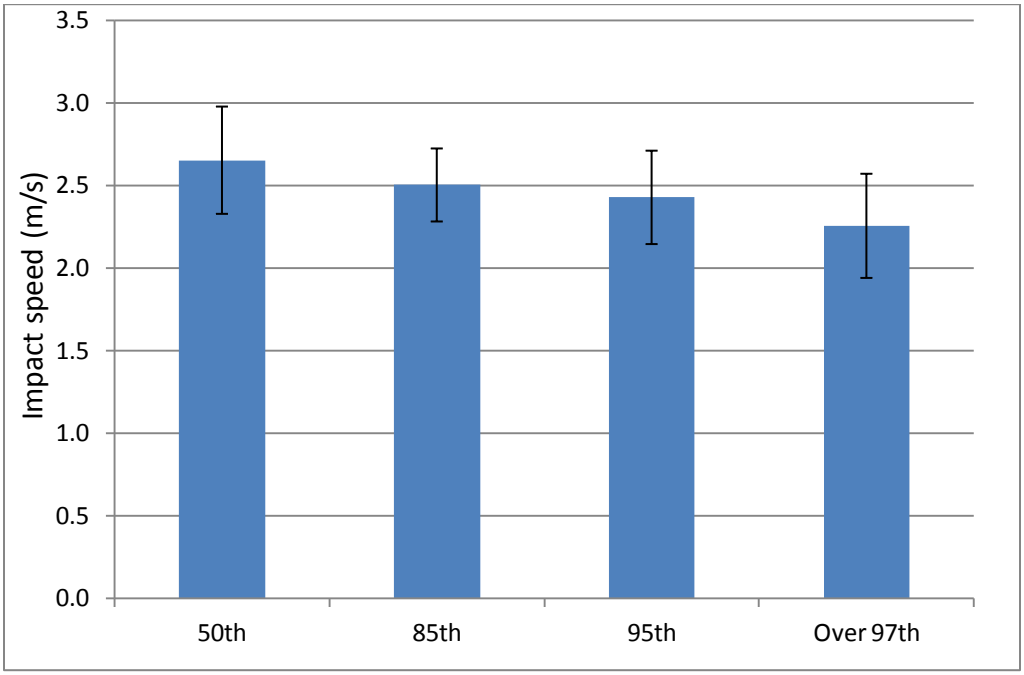

Figure 25. The mean values and standard deviations of the critical speeds in the full body model.

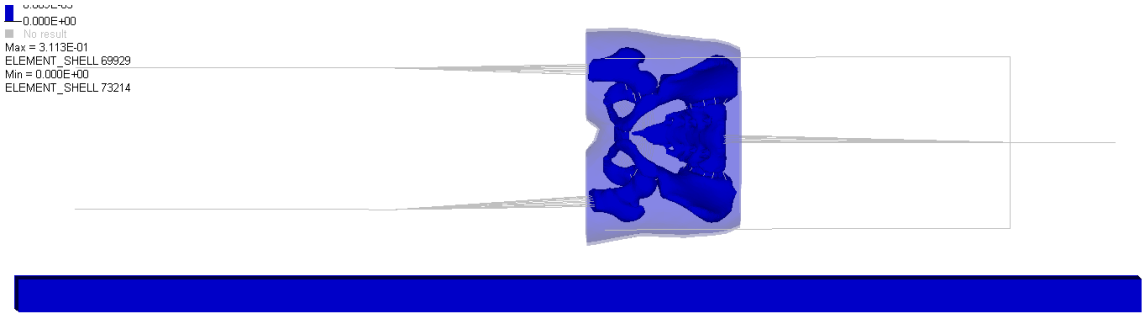

0 ms

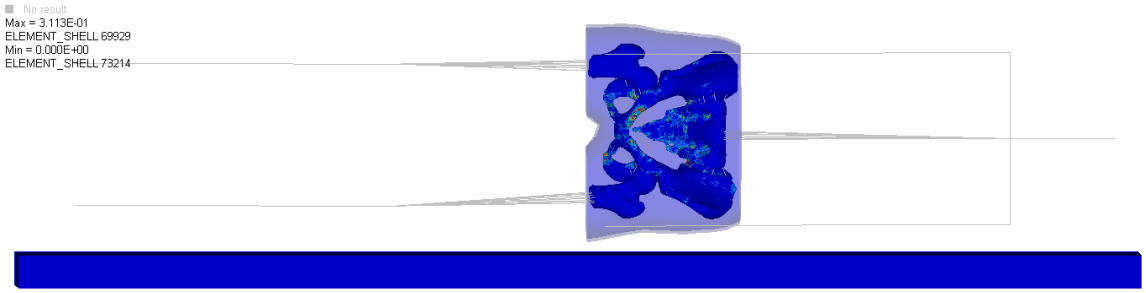

10 ms

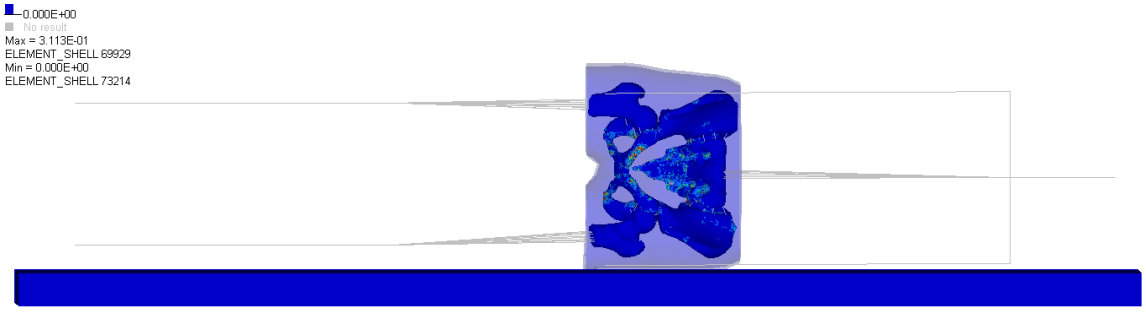

20 ms

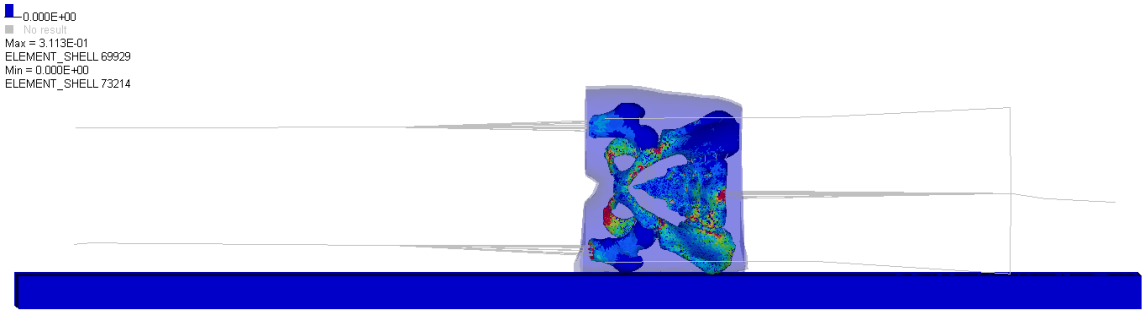

30 ms

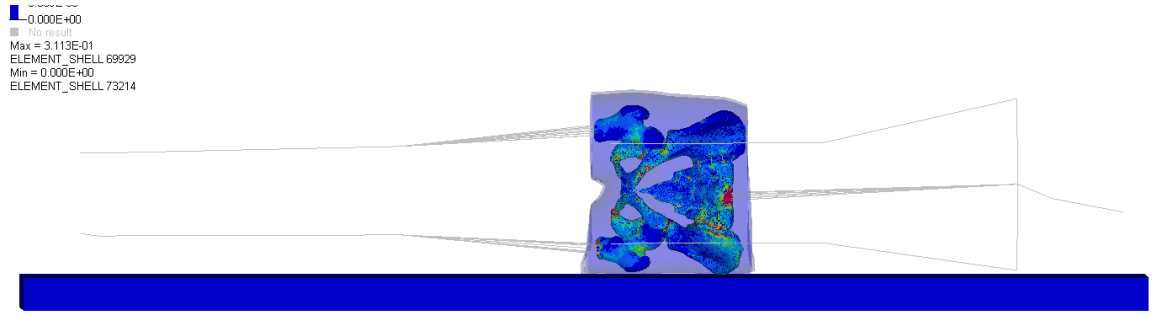

40 ms

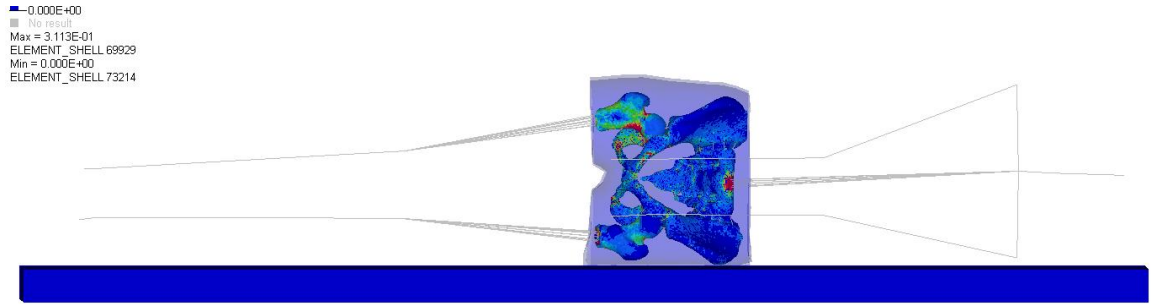

50 ms

Figure 26. A series of snapshots of the full body movement of the 50th percentile model.

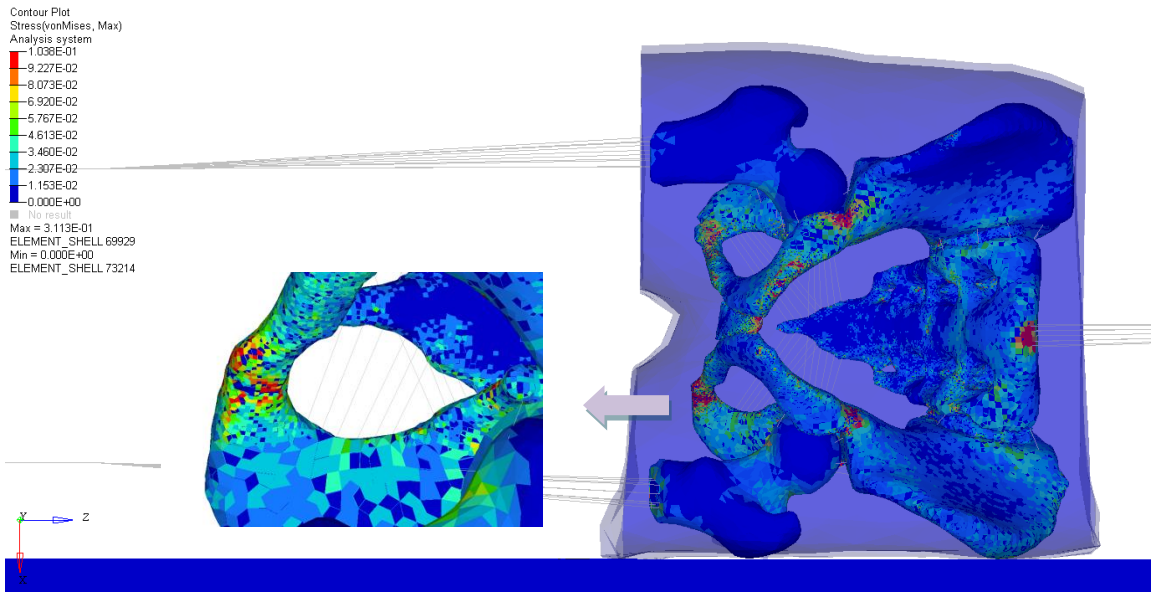

Figure 27. A snapshot of sideways fall simulation and bone fracture. Color contour indicates von-Mises stress.

CHAPTER 4

DISCUSSION AND CONCLUSION

To tackle the challenging physiological issue regarding the effect of obesity in pelvis injury, this study investigated the risk of pelvic bone fracture by addressing the level of obesity, in particular, childhood obesity. To monitor the responses and to examine pelvis fracture conditions in terms of obesity, three-dimensional (3D) finite element models and computational method were exploited to realize sideways falls. This approach provided an efficient way to the research of body injury of obese individuals. Two sets of models, body component models and full body models, were developed and tested. Sensitivity analysis was conducted to identify material parameters that substantially affected the model responses.

Discussion

In this study, pelvis-femur complex model and simple full body model offered a comparison between cushion effect and momentum effect on the risk of bone fracture. From the result of pelvis-femur complex simulation in Figure 18, the cushion effect of the SAT was observed. In Figures 18a and 18b, the curves of impact force and viscous criteria became wider, and the peaks of impact force and viscous criteria were decreased as SAT thickness increased. The absorbed strain energy (Figure 18c) was increased as obesity level increased. These results pointed out the cushion effect of the SAT.

Not only did the soft tissues absorb impact energy, but also the bone absorbed a certain amount of energy as shown in Table 7. Through Table 7, the inferior pubic ramus on the impact side had the highest stress. Also, both sides of superior pubic ramus and ischial tuberosity, and inferior pubic ramus of the contralateral side showed relatively high stresses. These hot spots are more likely to be subject to injury if the impact force is increased. As the result of critical impact speed shown in Figure 21, the critical impact speed increased slightly as the obesity level increased. The trend in the end becomes smooth, which may present the limitation of cushion effect. A softer floor increased the critical impact speed as a result of the cushion effect of the floor (Figure 20).

The momentum effect of the full body mass was accounted as well as the cushion effect of the SAT in the full body simulation. The curves of impact force and viscous criteria became wider (Figures 23a and 23b), which was similar to the pelvis-femur complex case. The strain energy absorbed by the SAT (Figure 23c) was increased as obesity increased. However, in contrast to pelvis-complex cases, the peaks of impact force and viscous criteria were increased as the BMI increased. This result indicated that the cushion effect of SAT was still observed, but the momentum effect of the body mass is more significant than the cushion effect.

In Table 8, the inferior pubic ramus on the impact side also had the highest stress while impacted. Both sides of the femoral neck were the second highest stressed spots. This may be a result of taking the inertia of the lower extremity in to consideration. The critical impact speed in the full body simulation decreased significantly as obesity increased (Figure 25). The outcome implies that the pelvic bone of obese children would be fractured at a certain impact speed; however, this is not true for children of average

size at the same impact speed. The inferior pubic ramus fracture in full body simulation was also observed. A softer floor increased the critical impact speed as a result of the cushion effect of the floor.

As expected from the results of the stress distribution, the inferior pubic ramus on the impact side was fractured at the critical impact speed, which is the most common fracture location during pelvic side impact as seen in the literature. For instance, lateral compression caused pubic remus oblique fracture [38]. Silber and Flynn [39] pointed out that 53% children with an immature pelvis (average age is around 5.7 years) had higher risk of pubic rami fracture. Arbogast et al. [40] revealed that the major fracture injury mechanisms in side impact collision for 8-11 year-old children was isolated pubic rami fractures. The results of simulation are consistent with the findings in the literature.

Limitations

There are a couple of limitations in this study.

1. All models utilized the same size HST layer. The volume of HST may be variable with different levels of obesity, but this study focused on the effect of various thicknesses of SAT and body mass on bone fracture risk. Further study is to exploit magnetic resonance imaging (MRI) data and other relevant data to establish different sizes and properties of the HST portion to improve the accuracy of simulation models.
2. All beam elements which were used to present different components were assumed as cylinders. In order to imitate the dynamic movement of each body component in modeling, not only length and mass distribution should be considered, but also the

shape and the center of mass of each body part have to be concerned. An improvement is to develop a full body FE model based on a CT scan from a full body child imaging data. The result of simulation then will be more reliable.

3. The same bone properties were applied to all the models. Goulding et al. [41] reported that overweight and obese children have lower bone mineral density and lower bone mass and area for their weight. Rocher et al. [42] also observed that whole body bone mineral apparent density was lower in obese children. On the contrary, Leonard et al. [43] concluded that greater whole body bone area and bone mineral content for age were associated with obesity. Ellis et al. [44] concluded obese children do not have lower whole body bone mineral content as well. If the relationship between bone density and obesity level is clarified, the results would be more credible.
4. The pelvis fracture pattern of children and adolescents may be different from adults. Dellorusso [45] indicated that the exceptions of child bone fracture involve growth plates. When an injury occurs in children near a growth plate, the impact force will lead to a fracture of the growth plate. The growth plate of the femur is located close to the femur neck. According to the maximum stress distribution in Table 8, the femur necks (measuring spots 4 and 16) showed higher stresses. Thus, the material properties and the structure of femur growth plate will be considered in the further study. The direction of impact force is another interesting topic which may discover the critical impact angle for children pelvis.

Conclusion

In conclusion, in sideways fall simulations, the momentum effect of a greater body mass is more significant than the cushion effect of the trochanteric SAT layer. Therefore, under the same impact speed, obese children will have higher risk of bone fracture than average size children. A further implication is that obese children may need different criteria for all kinds of protection devices.

LIST OF REFERENCES

1. Ogden, C., Carroll, M., 2010. Prevalence of obesity among children and adolescents: United States, trends 1963-1965 through 2007-2008. Division of Health and Nutrition Examination Surveys.

2. Kuczmarski, R.J., Ogden, C.L., Guo, S.S., et al., 2000. CDC growth charts for the United States: methods and development. Vital Health Stat 11(246), 1-190.

3. Courtney, A.C., Wachtel, E.F., Myers, E.R., Hayes, W.C., 1994. Effect of loading rate on strength of the proximal femur. Calcified Tissue International 55, 53-58

4. Hayes, W.C., Myers, E.R., Robinovitch, S.N., van den Kroonenberg, A.J., Courtney, A.C., McMahon, T.A., 1996. Etiology and prevention of age-related hip fractures. Bone 18(Suppl. 1), 77S-86S.

5. Bouxsein, M.L., Szulc, P., Munoz, F., Thrall, E., Sornay-Rendu, E., Delmas, P.D., 2007. Contribution of trochanteric soft tissues to fall force estimates, the factor of risk, and prediction of hip fracture risk. Journal of Bone and Mineral Research 22, 825-831.

6. Majumder, S., Roychowdhury, A., Pal, S., 2008. Effects of trochanteric soft tissue thickness and hip impact velocity on hip fracture in sideways fall through 3D finite element simulations. Journal of Biomechanics 41(13), 2834-2842.

7. van den Kroonenberg, A.J., Hayes, W.C., McMahon, T.A., 1996. Hip impact velocities and body configurations for voluntary falls from standing height. Journal of Biomechanics 29(6), 807-811.

8. Davidson, P.L., Goulding, A., Chalmers, D.J., 2003. Biomechanical analysis of arm fracture in obese boys. Journal of Paediatrics and Child Health 39(9), 657-664.

9. Pollack, K.M., Xie, D., Arbogast, K.B., Durbin, D.R., 2008. Body mass index and injury risk among US children 9–15 years old in motor vehicle crashes. Injury Prevention 14(6), 366-371.

10. Pomerantz, W.J., Timm, N.L., Gittelman, M.A., 2010. Injury patterns in obese versus nonobese children presenting to a pediatric emergency department. Pediatrics 125(4), 681-685.

11. Timm, N.L., Grupp-Phelan, J., Ho, M.L., 2005. Chronic ankle morbidity in obese children following an acute ankle injury. Archives of Pediatrics Adolescent Medicine 159(1),33-36.

12. Bazelmans, C., Coppieters, Y., Godin, I., Parent, F., Berghmans, L., Dramaix, M., Levêque, A., 2004. Is obesity associated with injuries among young people? European Journal of Epidemiol 19(11), 1037-1042.

13. Kim, J.E., Li, Z., Ito, Y., Huber, C.D., Shih, A., Eberhardt, A.W., Yang, K.H., King, A.I., Soni, B.K., 2009. Finite element model development of a child pelvis with optimization-based material identification. Journal of Biomechanics 42(13), 2191-95.

14. Kikuchi, Y., Takahashi, Y., Mori, F., 2006. Development of a finite element model for a pedestrian pelvis and lower limb. SAE Technical Paper 2006-01-0683. doi:10.4271/2006-01-0683.

15. Li, Z., Alonso, J.E., Kim, J.E., Davidson, J.S., Etheridge, B.S., Eberhardt, A.W., 2006. Three-dimensional finite element models of the human pubic symphysis with viscohyperelastic soft tissues. Annals of Biomedical Engineering 34(9), 1452-1462.

16. Anderson, A.E., Peters, C.L., Tuttle, B.D., Weiss, J.A., 2005. Subject-specific finite element model of the pelvis: development, validation and sensitivity studies. Journal of Biomechanical Engineering 127(3), 364-373.

17. Dakin, G.J., Arbelaez, R.A., Molz, F.J., Alonso, J.E., Mann, K.A., Eberhardt, A.W., 2001. Elastic and viscoelastic properties of the human pubic symphysis joint: effects of lateral impact loading. Journal of Biomechanical Engineering 123(3), 218-226.

18. Li, Z., Kim, J.E., Davidson, J.S., Etheridge, B.S., Alonso, J.E., Eberhardt, A.W., 2007. Biomechanical response of the pubic symphysis in lateral pelvic impacts: a finite element study. Journal of Biomechanics 40(12), 2758-2766.

19. Hewitt, J., Guilak, F., Glisson, R., Vail, T.P., 2001. Regional material properties of the human hip joint capsule ligaments. Journal of Orthopaedic Research 19(3), 359-364.

20. Phillips, A.T.M., Pankaj, P., Howie, C.R., Usmani, A.S., Simpson, A.H.R.W., 2007. Finite element modeling of the pelvis: Inclusion of muscular and ligamentous boundary conditions. Medical Engineering & Physics 29(7), 739-748.

21. Agache, P,, Monneur, C., Leveque, J.L., De Rigal, J., 1980. Mechanical properties and Young's modulus of human skin in vivo. Archives of Dermatological Research 269, 221-232.

22. Zheng, Y., Mak, A.F.T., Lue, B., 1999. Objective assessment of limb tissue elasticity: Development of a manual indentation procedure. Journal of Rehabilitation Research and Development 36(2), 71-85.

23. Seidenari, S., Giusti, G., Bertoni, L., Magnoni, C., Pellacani, G., 2000. Thickness and echogenicity of the skin in children as assessed by 20-MHz ultrasound. Dermatology 201(3), 218-222.

24. Alekseev, S.I., Radzievsky, A.A., Logani, M.K., Ziskin, M.C., 2008. Millimeter wave dosimetry of human skin. Bioelectromagnetics 29(1), 65-70.

25. Todd, B.A., Thacker, J.G., 1994. Three-dimensional computer model of the human buttocks in vivo. Journal of Rehabilitation Research and Development 31(2), 111-119.

26. Fidanza, F., Keys, A., Anderson, J.T., 1953. Density of body fat in man and other mammals. Journal of Applied Physiology 6, 252-256.

27. Vannah, W.M., Childress, D.S., 1996. Indentor tests and finite element modeling of bulk muscular tissue in vivo. Journal of Rehabilitation Research and Development 33(3), 239-252.

28. Ouyang, J., Zhu, Q., Zhao, W., Xu, Y., Chen, W., Zhong, S., 2003. Experimental cadaveric study of lateral impact of the pelvis in children. Academic Journal of the First Medical College of PLA 23(5), 397-408.

29. Hallquist J.O., 1998. LS-DYNA3D Theoretical Manual. Livermore, CA Livermore Software Technology Corporation.

30. McDowell, M.A., Fryar, C.D., Ogden, C.L., et al., 2008. Anthropometric reference data for children and adults: United States, 2003–2006. National Health Statistics Report No. 10. National Center for Health Statistics.

31. Yokoi, T., Shibukawa, K., Ae, M., 1986. Body segment parameters of Japanese children. Japan Journal of Physical Education 31, 53-66. http://www.dh.aist.go.jp/bodyDB/m/e-k-07.html

32. Bauer, J.J., Pavol, M.J., Snow, C.M., et al., 2007. MRI-derived body segment parameters of children differ from age-based estimates derived using photogrammetry. Journal of Biomechanics 40, 2904-2910.

33. Ganley, K.J., Powers, C.M., 2004. Anthropometric parameters in children: a comparison of values obtained from dual energy X-ray absorptiometry and cadaver-based estimates. Gait Posture 19, 133-140.

34. de Leva P., 1996. Adjustments to Zatsiorsky-Seluyanov's segment inertia parameters. Journal of Biomechanics 29, 1223-1230.

35. Majumder, S., Roychowdhury, A., Pal, S., 2007. Simulation of hip fracture in sideways fall using a 3D finite element model of pelvis-femur-soft tissue complex with simplified representation of whole body. Medical Engineering & Physics 29(10), 1167-1178.

36. Crandall, S.H., Dahl, N.C., Lardner, T.J., 1999. An introduction to the mechanics of solids: Second edition with SI units. New York, NY: McGraw-Hill.

37. Keyak, J.H., Rossi, S.A., 2000. Prediction of femoral fracture load using finite element models: an examination of stress- and strain-based failure theories. Journal of Biomechanics 33(2), 209-214.

38. Young, J.W.A., Burgess, A.R., 1987. Radiologic management of pelvic ring fractures. Baltimore: Urban & Schwartzenberg.

39. Silber, J.S., Flynn, J.M., 2002. Changing patterns of pediatric pelvis fractures with skeletal maturation: implications for classification and management. Journal of Pediatric Orthopaedics 22(1), 22-26.

40. Arbogast, K.B., Mari-Gowda, S., Kallan, M.J., Durbin, D.R., Winston, F.K., 2002. Pediatric pelvic fractures in side impact collisions. Stapp Car Crash Journal 46, 285-296.

41. Goulding, A., Taylor, R.W., Jones, I.E., McAuley, K.A., Manning, P.J., Williams, S.M., 2000. Overweight and obese children have low bone mass and area for their weight. International Journal of Obesity 24, 627-632.

42. Rocher, E., Chappard, C., Jaffre, C., Benhamou, C.L., Courteix, D., 2008. Bone mineral density in prepubertal obese and control children: relation to body weight, lean mass, and fat mass. Journal of Bone and Mineral Metabolism 26(1), 73-78.

43. Leonard, M.B., Shults, J., Wilson, B.A., Tershakovec, A.M., Zemel, B.S., 2004. Obesity during childhood and adolescence augments bone mass and bone dimensions. The American Journal of Clinical Nutrition 80,514 –523.

44. Ellis, K.J., Shypailo, R.J., Wong, W.W., Abrams, S.A., 2003. Bone mineral mass in overweight and obese children: diminished or enhanced? Acta Diabetologica 40(Suppl. 1), S274-S277.

45. Dellorusso, B., 2012. Pediatric Pelvis Fractures. Journal of Trauma & Treatment 1(3), 1-6.

APPENDIX

SERIES OF CAPTURED IMAGES IN SIDEWAYS FALL

Case Study 1-2. TST = 8.6 mm on rigid floor with bone fracture, v = 3.9 m/s.

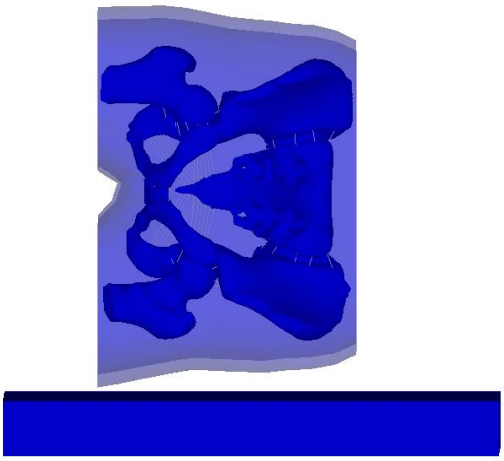

0 ms

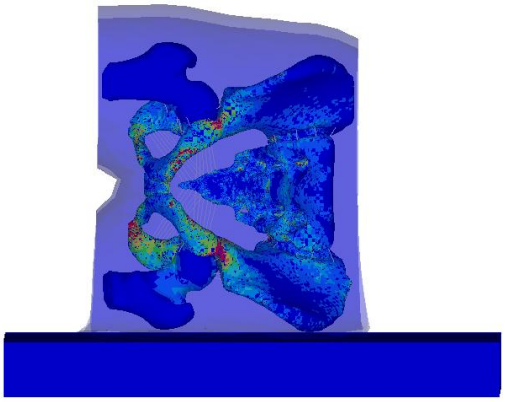

10 ms

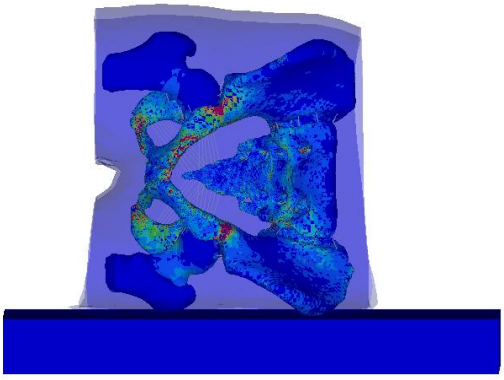

20 ms

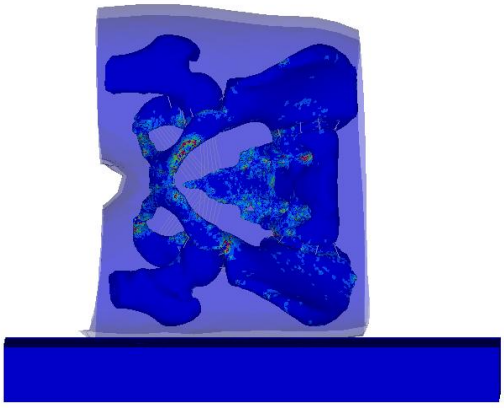

30 ms

Case Study 1-3. TST = 16.3 mm on rigid floor with bone fracture, v = 4.1 m/s.

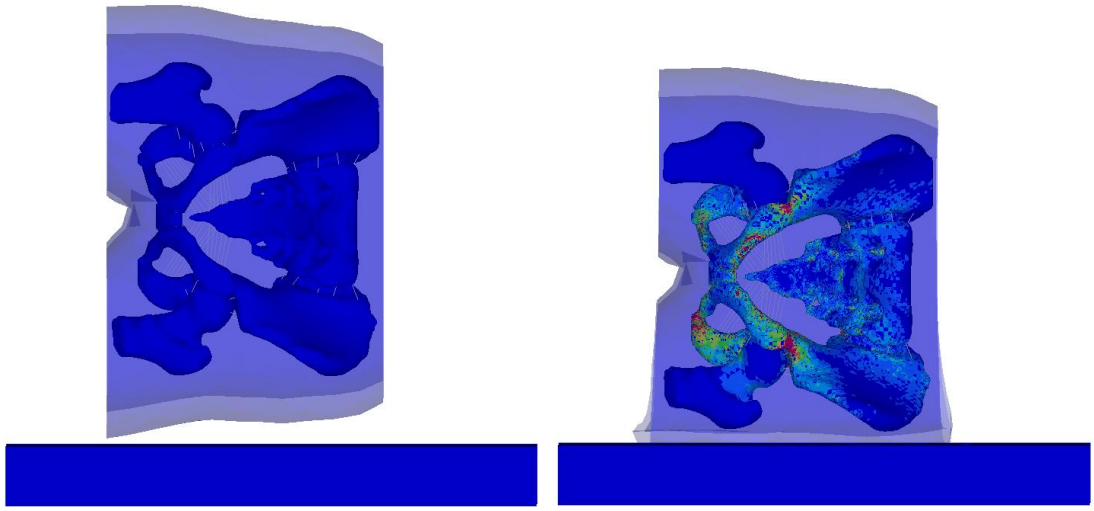

0 ms

10 ms

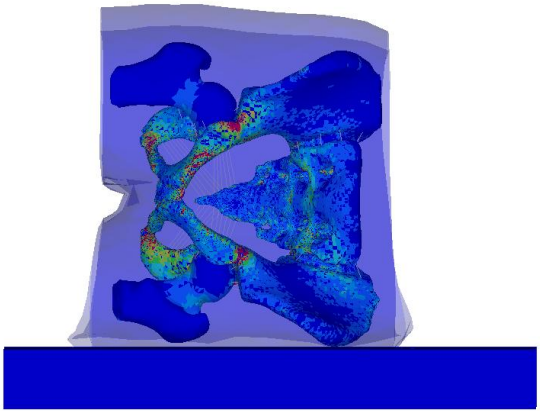

20 ms

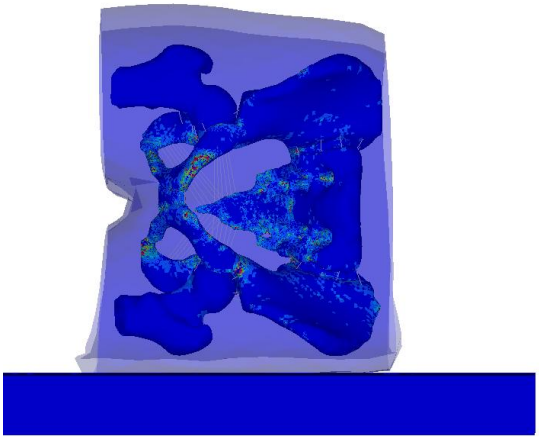

30 ms

Case Study 1-4. TST = 24.7 mm on rigid floor with bone fracture, v = 4.1 m/s.

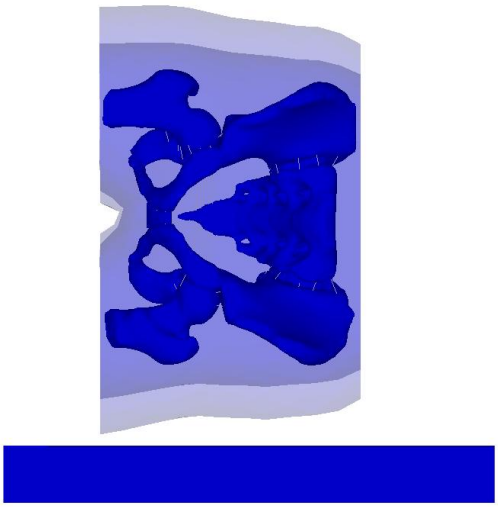

0 ms

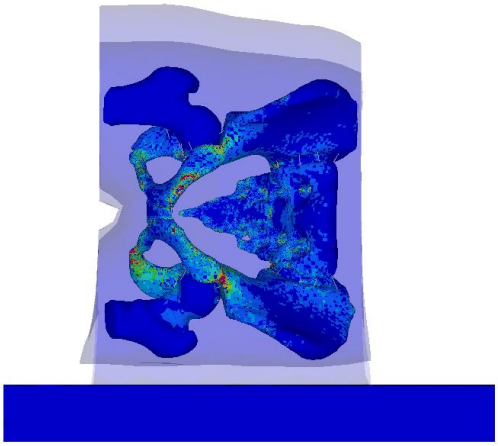

10 ms

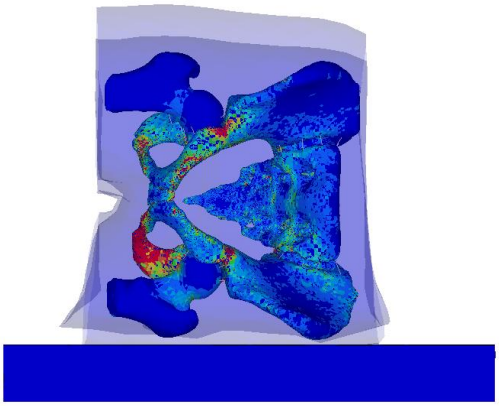

20 ms

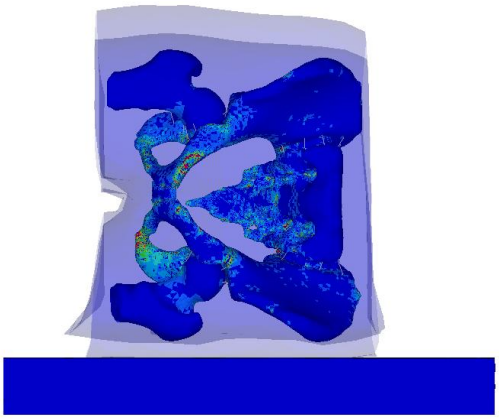

30 ms

Case Study 5-2. 85th percentile on rigid floor with bone fracture, v = 2.3 m/s.

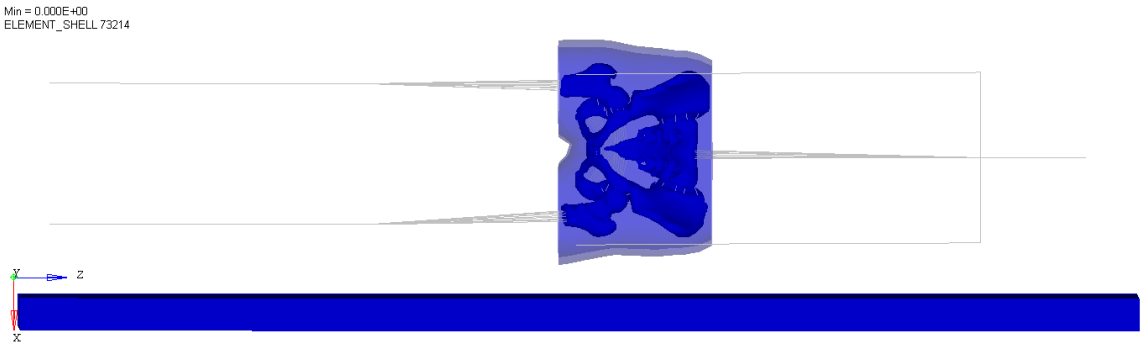

0 ms

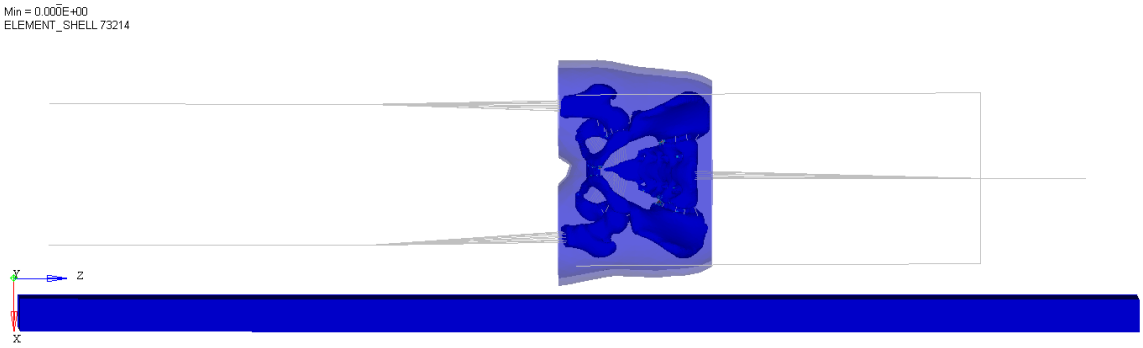

10 ms

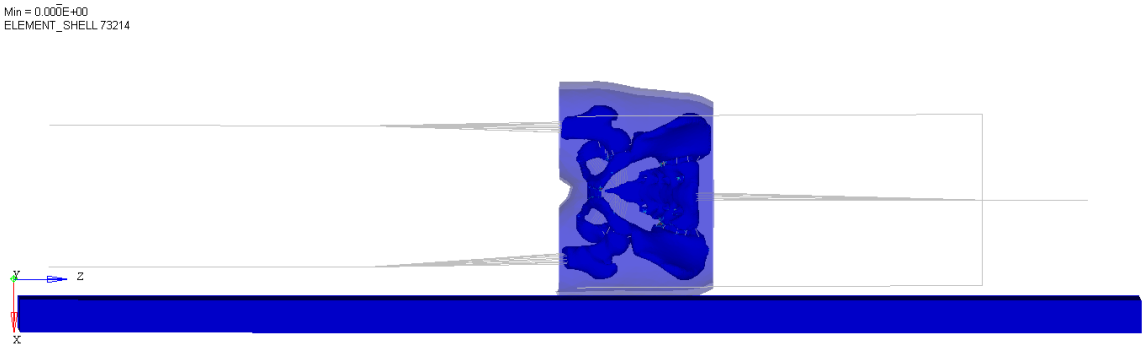

20 ms

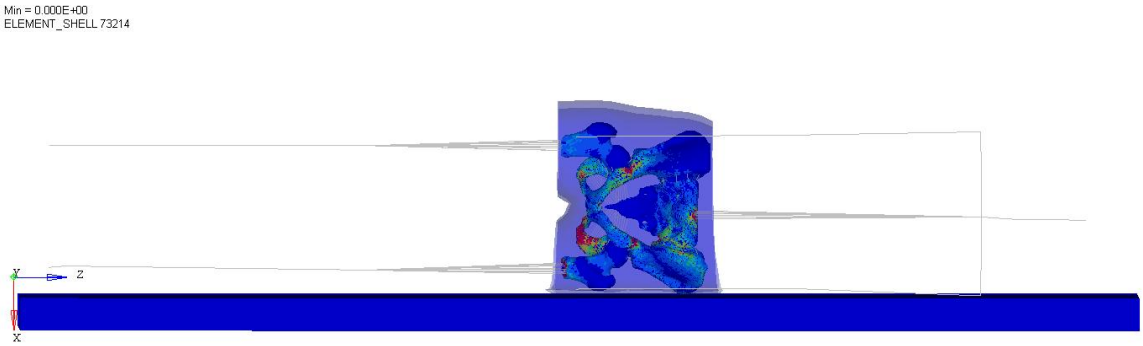

30 ms

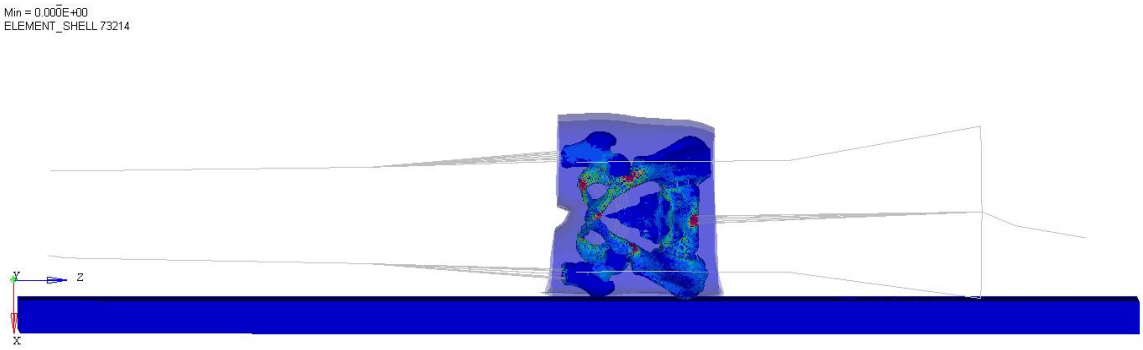

40 ms

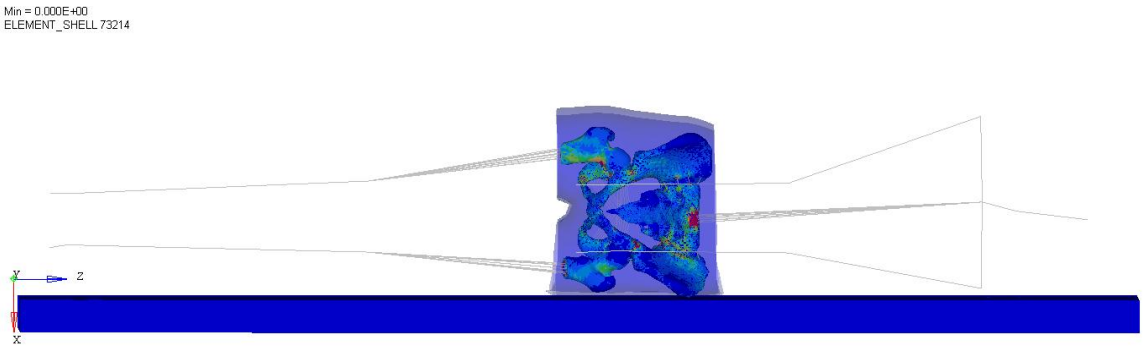

50 ms

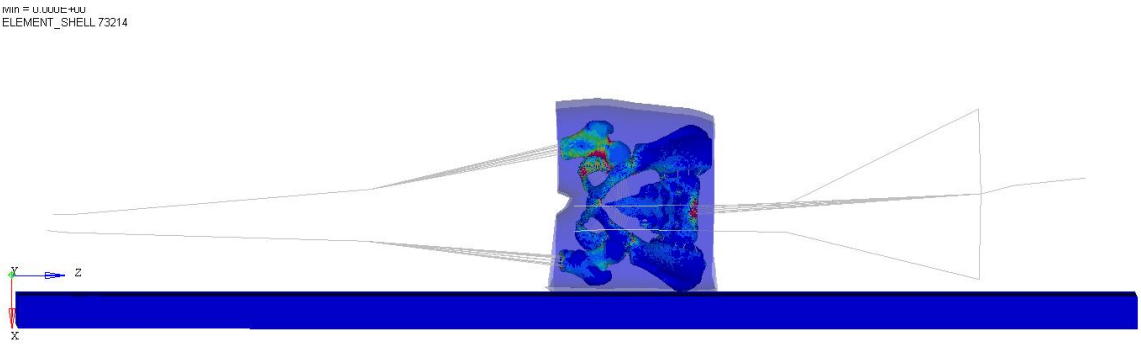

60 ms

Case Study 5-3. 95th percentile on rigid floor with bone fracture, v = 2.105 m/s.

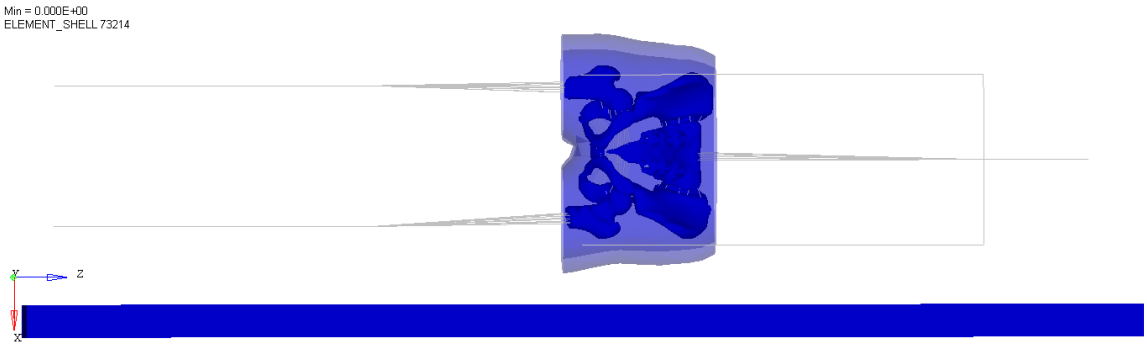

0 ms

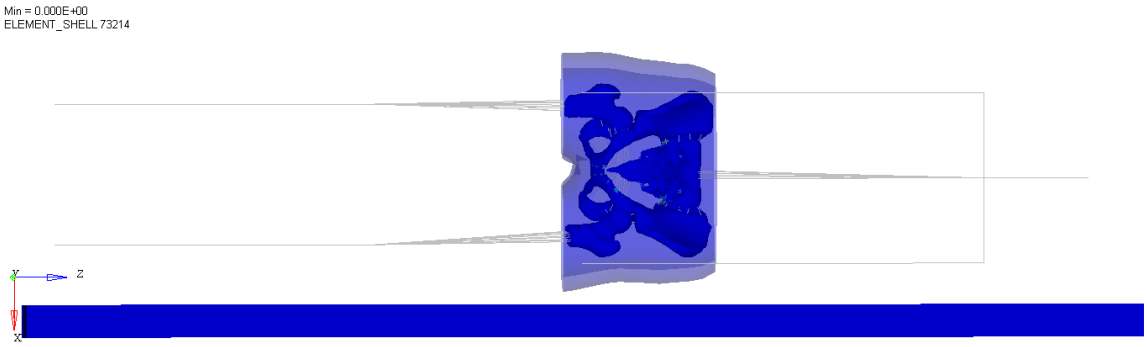

10 ms

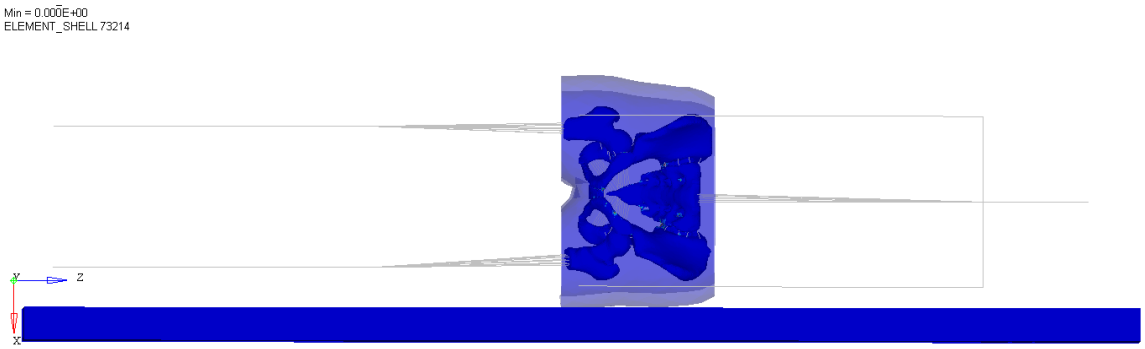

20 ms

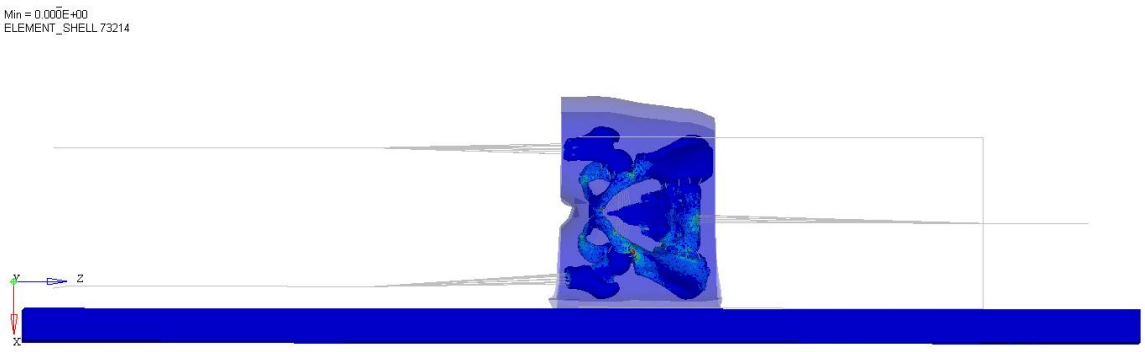

30 ms

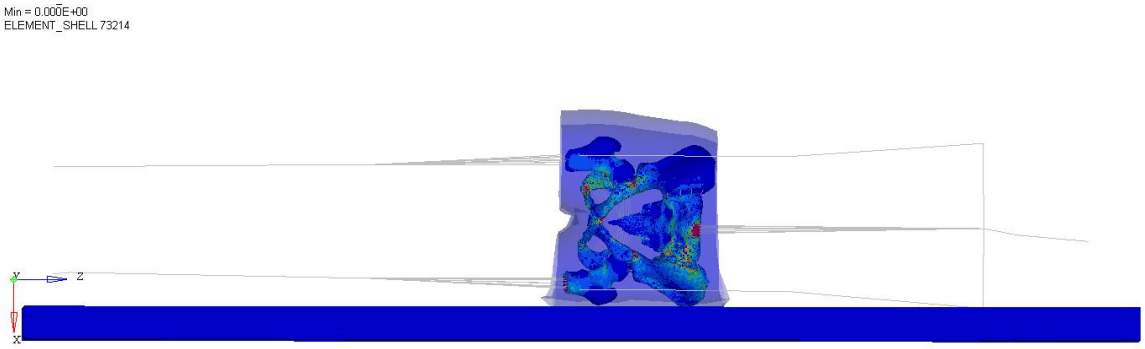

40 ms

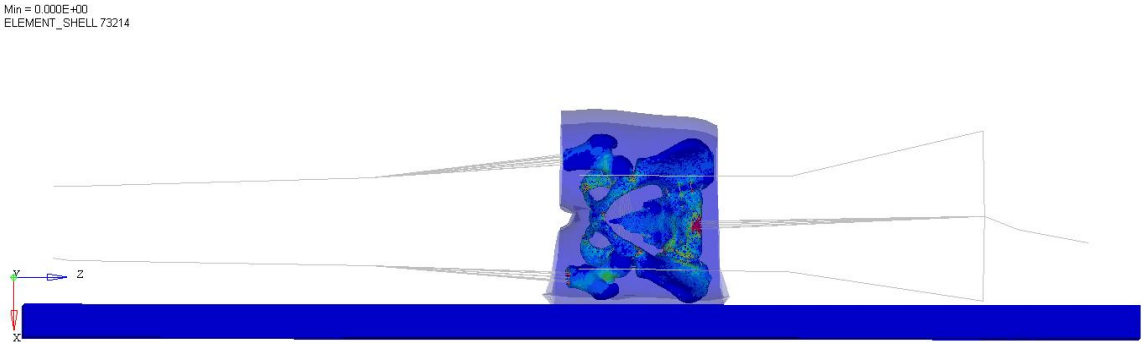

50 ms

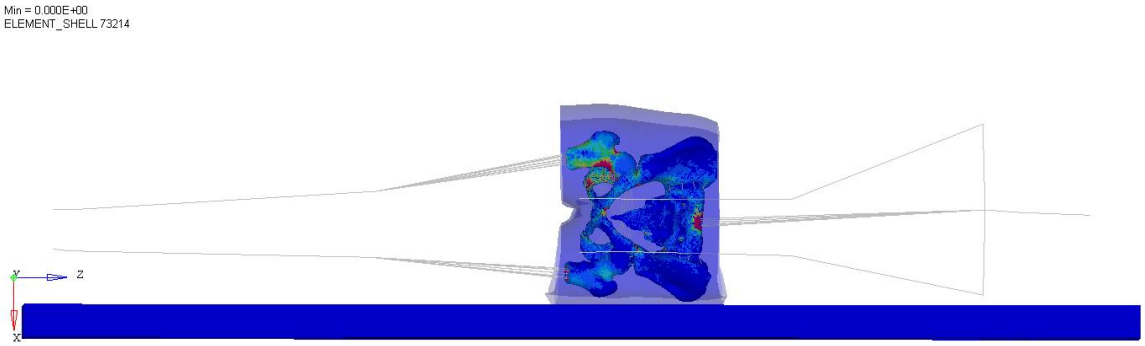

60 ms

Case Study 5-4. 97th percentile on rigid floor with bone fracture, v = 1.84 m/s.

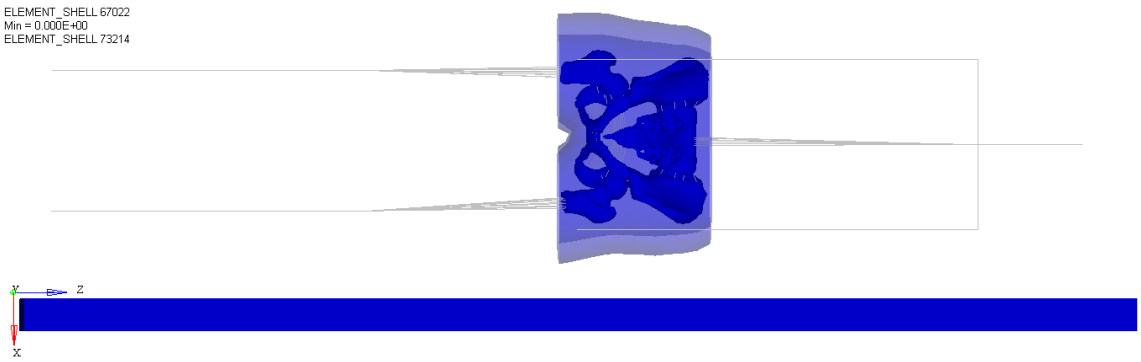

0 ms

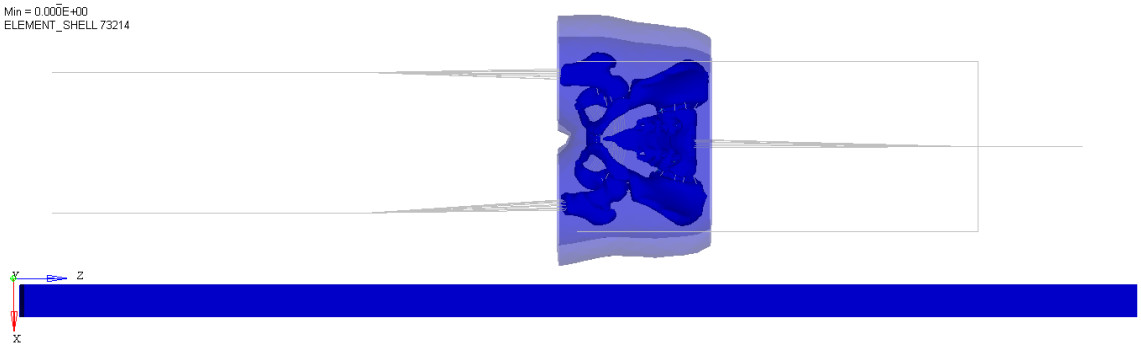

10 ms

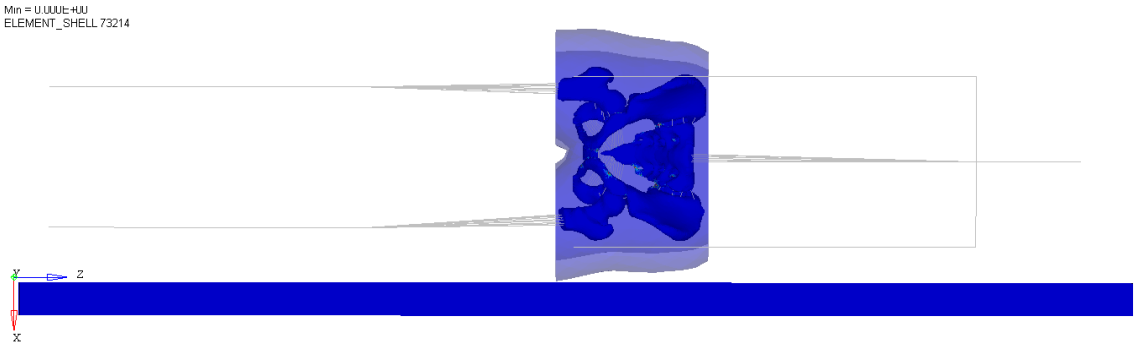

20 ms

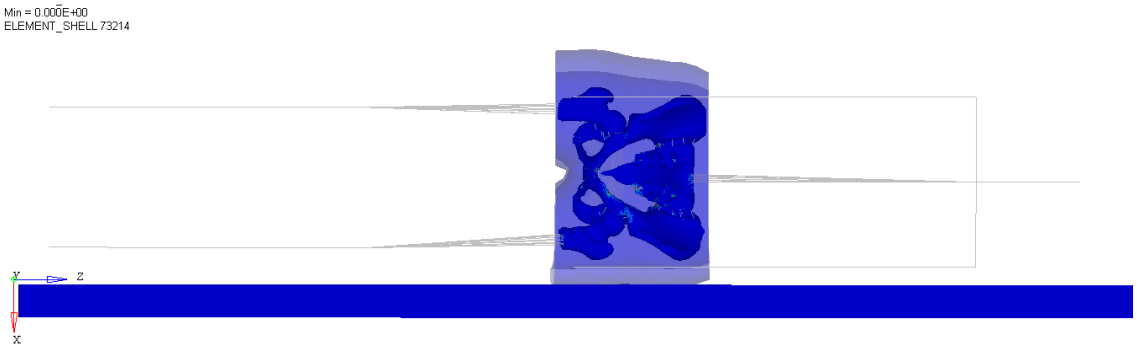

30 ms

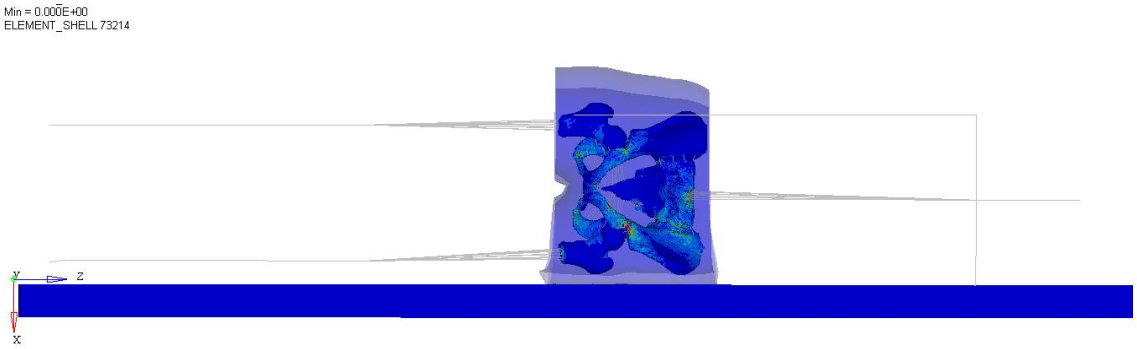

40 ms

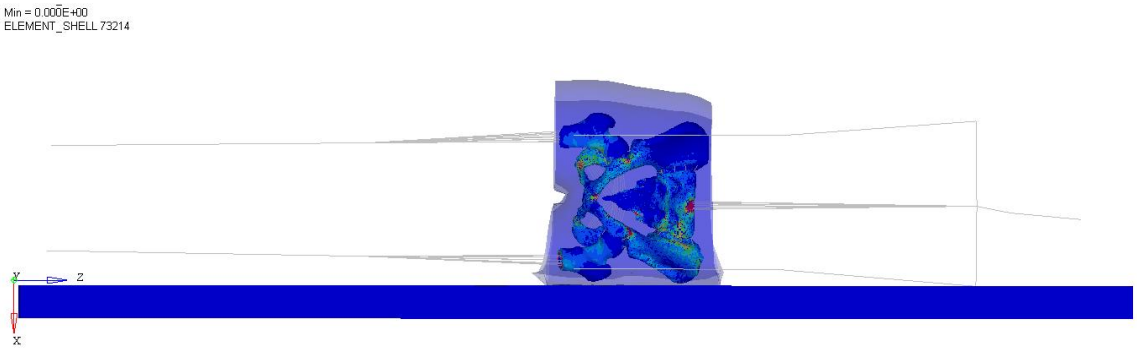

50 ms

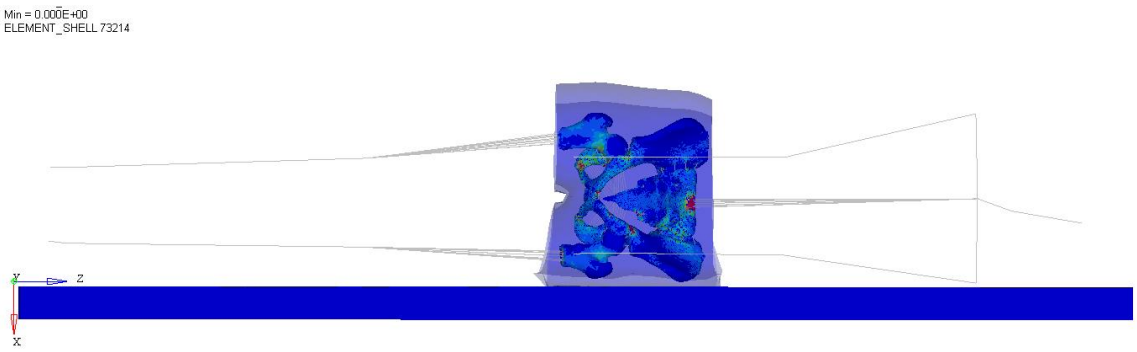

60 ms